DESIGN OF A HIGH TEMPERATURE EROSION APPARATUS FOR TESTING OF BOILER TUBES

A THESIS SUBMITTED TO
THE GRADUATE SCHOOL OF NATURAL AND APPLIED SCIENCES
OF
MIDDLE EAST TECHNICAL UNIVERSITY

BY

HÜSEYİN ERGÜN

IN PARTIAL FULFILLMENT OF THE REQUIREMENTS
FOR
THE DEGREE OF MASTER OF SCIENCE
IN
METALLURGICAL AND MATERIALS ENGINEERING

OCTOBER 2010

Approval of the thesis:

DESIGN OF A HIGH TEMPERATURE EROSION APPARATUS FOR TESTING OF BOILER TUBES

submitted by **HÜSEYİN ERGÜN** in partial fulfillment of the requirements for the degree of **Master of Science in Metallurgical and Materials Engineering Department, Middle East Technical University** by

Prof. Dr. Canan Özgen _____
Dean, Graduate School of Natural and Applied Sciences

Prof. Dr. Tayfur Öztürk _____
Head of Department, Metallurgical and Materials Eng.

Prof. Dr. Tayfur Öztürk _____
Supervisor, Metallurgical and Materials Eng. Dept., METU

Prof. Dr. Mustafa Doruk _____
Co-Supervisor, Metallurgical and Materials Eng. Dept., METU

Examining Committee Members

Prof. Dr. Tayfur Öztürk _____
Metallurgical and Materials Eng. Dept., METU

Prof. Dr. Mustafa Doruk _____
Metallurgical and Materials Eng. Dept., METU

Prof. Dr. Kadri Aydınol _____
Metallurgical and Materials Eng. Dept., METU

M.Sc. Nurettin Savruk _____
Elektrik Üretim A.Ş. Genel Müdürlüğü

M.Sc. Mücella Ersoy _____
Türkiye Kömür İşletmeleri Kurumu Genel Müdürlüğü

Date: 16 /09/2010

I hereby declare that all information in this document has been obtained and presented in accordance with academic rules and ethical conduct. I also declare that, as required by these rules and conduct, I have fully cited and referenced all material and results that are not original to this work.

Name, Last name: Hüseyin ERGÜN

Signature :

ABSTRACT

DESIGN OF A HIGH TEMPERATURE EROSION APPARATUS FOR TESTING OF BOILER TUBES

Ergün, Hüseyin

M.Sc., Department of Metallurgical and Materials Engineering

Supervisor: Prof. Dr. Tayfur Öztürk

Co-supervisor: Prof. Dr. Mustafa Doruk

October 2010, 58 pages

In this thesis an apparatus is designed which enables the testing of thermal power plant boiler tubes against erosion. The apparatus makes use of a tube sample directly cut from the boiler tubes and simulates conditions similar to those prevailing in boilers in lignite fired power plants. The apparatus is composed of three components; a furnace for heating the sample, a loading system which allows application of tensile stresses while allowing the rotation of the sample, and a particle blower that delivers abrasive particles to the surface of the sample. The abrasive material used in the test is mixture of oxides, 90% of which is Al_2O_3 and the average particle size is approximately 300 μm. The unit as designed would allow testing of boiler tubes up to a temperature of 650^{o}C, and particle velocity of up to 50 m/s. The apparatus as tested at room temperatures for four identical samples have yielded very similar erosion values based on measurement of weight loss. At elevated temperature, erosion could be measured by a thickness loss since the oxidation that occurs complicates the erosion measurement. Two economizer material; P235GH and

16Mo3 were tested at 500^{o}C with particle velocity of 10 m/s. The testing has shown that 16Mo3 has better performance than P235GH, the erosion rate differing by 20 percent.

Keywords: Boiler tubes, Erosion, Economizer, Thermal power plant

ÖZ

TERMİK SANTRAL KAZAN BORULARININ TESTİ İÇİN BİR YÜKSEK SICAKLIK AŞINMA TESTİ DÜZENEĞİ TASARIMI

Ergün, Hüseyin

Yüksek Lisans, Metalurji ve Malzeme Mühendisliği Bölümü

Tez Yöneticisi: Prof. Dr. Tayfur Öztürk

Ortak Tez Yöneticisi: Prof. Dr. Mustafa Doruk

Ekim 2010, 58 sayfa

Bu çalışmada termik santral kazan borularının aşınmaya karşı test edilebilmesine olanak sağlayan bir deney düzeneği geliştirilmiştir. Düzenek kazan borularından kesilmiş numuneleri kullanmakta ve linyitle çalışan termik santral kazan koşullarını canlandırmaktadır. Cihaz numunenin dönmesini sağlarken aynı zamanda çekme gerilimi uygulayan bir yükleme sistemi, numuneyi ısıtmak için bir fırın ve aşındırıcı parçacıkları numune yüzeyine gönderen parçacık püskürtücü olmak üzere üç ana kısımdan oluşmaktadır. Testlerde aşındırıcı parçacıklar olarak %90 oranında Al_2O_3 içeren ortalama parçacık boyutu 300μm mertebesinde bir oksit karışım kullanılmıştır. Sistem en çok 650^oC sıcaklığa ve 50 m/s parçacık hızlarına kadar test yapılabilinmesine olanak sağlamaktadır. Düzenek dört aynı özellikte numune ile, ağırlık kaybı ölçülmek sureti ile test edilmiş ve tekrarlanabilir sonuçlar verdiği ortaya konmuştur. Yüksek sıcaklıklarda aşınma, oksitlenmenin ölçümleri zorlaştırması nedeniyle kalınlık kaybı ile değerlendirilmiştir. Ekonomizer bölgesi için P235GH ve 16Mo3 malzemeleri 500^oC de 10 m/s hızla test edilmiş yapılan test sonucunda

16Mo3'ün P235GH'dan %20 aşınma hızı farkı ile daha iyi performans gösterdiğini tespit edilmiştir.

Anahtar Kelimeler: Erozyon, Ekonomizer, Kazan boruları, Termik santral

To my family and Öznur…

ACKNOWLEDGEMENTS

I would like to express my deepest gratitude to my supervisor Prof. Dr. Tayfur Öztürk, co-supervisor Prof. Dr. Mustafa Doruk and Prof. Dr. kadri Aydınol for their guidance, criticism and continuous support throughout the course of this thesis.

I would like to thank Oğuz Özgören EÜAŞ, and to the employees of Çayırhan, Çatalağzı, Yatağan, Kemerköy and Yeniköy thermal power plants for their help during the collection of data on the boiler tube failures. I would also like to thank to the personel of Metallurgical and Materials Department, Cengiz Tan, Yusuf Yıldırım, Salih Türe, and Cemal Yanardağ for their help in the experimental part of this study. I am grateful to Serkan Şenyurt and Erkan Köse both employee of Öz-San AŞ where the test setup was constructed.

I wish to thank to design project group T7 of 2007 graduates who carried out the preliminary design of the test setup. I am also grateful to my friend and colleague Özgür Öztürk and also to Onur Rauf Bingöl, Sadık Bayramoğlu, Serdar Savaş and Göksu Gürer for their support for various aspects of this work.

Financial support for this study was provided by DPT (BAP-03-08-DPT-2007K120220) which I gratefully acknowledge.

TABLE OF CONTENTS

LIST OF TABLES

TABLES

LIST OF FIGURES

FIGURES

CHAPTER 1

INTRODUCTION

Coal fired thermal power plants continue to have a substantial share in power generation, i.e. 42% of the total [1]. They have also a significant share in the power generation in Turkey. According to 2009 annual sector report of Elektrik Üretim AŞ (EÜAŞ), 28% of the electricity was generated in coal fired thermal power plants [2]. The most of the coal reserves in Turkey are lignite with calorific values usually between 1000-2000 kcal/kg [3].

Low calorific lignite results in high fly ash content, which generally comprises Al_2O_3, SiO_2 and Fe_2O_3 [4]. The fly ash leads to erosion in boiler tubes especially in regions where they have high velocities. Thus, they may lead to failure of tubes resulting forced outage of the boiler.

Main failure modes observed in boiler tubes are erosion, short term overheating usually linked with deposit formation, creep (long term overheating), and corrosion. The laboratory reports of EÜAŞ [5] indicate that, the erosion make up 28% the total. This is followed by failures caused by short term overheating (deposit formation) 22%. These failures are observed mainly in the superheater, reheater and economizer regions of the boiler. Erosion failure arises mostly from fly ash which inside the boiler move with speeds in the order of 15-55 m/s. Fly ash erosion is quite dominant in economizer regions where the tube arrays have close spacing.

Forced outage of boiler leads to considerable loss of energy and the resources and there is considerable interest for minimizing or eliminating the failures mostly arises

in tubes. Thus, the testing of boiler tubes against failures has attracted considerable interest over the decades.

The current study deals with erosion failures with reference to tubes in economizer region of power plant. The work was undertaken to develop a test apparatus which can be used to test and evaluate the boiler tube materials against erosion.

CHAPTER 2

LITERATURE REVIEW

Coal fired power plants has a share of 42% in the electricity generation in the world as whole in 2007. According to EUAŞ [2], in 2009 the share is lower for Turkey making up only 28% of the total, greater portion of the remaining part is made up of power plants based on natural gas (49%). Three fourth of the coal fired power plants in Turkey make use of lignite. Lignite is the most important indigenous energy resource in Turkey with the estimated reserve of 11.5 billion tons. The lignite deposits are spread across the country, lignite deposits at Afşin-Elbistan being particularly noteworthy.

The power plants making use of lignite have a total capacity of 8079 MW in Turkey, **Table 2.1**. Additionally there are 2 domestic one hard coal (300 MW) and the other asphaltite (135 MW) and 3 imported hard coal power plants (1780 MW).

According to 2009 TKİ report [3] the calorific values of lignite reserve range between 1000-4200 kcal/kg. The 66% of these reserves have calorific value of 1000-2000 kcal/kg and 25% has calorific value of 2001-3000 kcal/kg. For instance, Afşin-Elbistan the lower calorific value is between 900-1250 kcal/kg.

2.1 Boiler in Coal Fired Power Plants

Figure 2.1 shows a diagram of a boiler in a conventional thermal power plant. The main components are i) furnace and evaparator ii) superheaters, iii) reheater, iv)

Table 2.1 Lignite fired thermal power plants in Turkey (TKİ, 2010) [3]

Project Name	**Coal Consumption**	**Power(MW)**
Muğla-Yatağan	5350	630
Muğla-Milas-Yeniköy	3750	420
Muğla-Hüsamlar-Kemerköy	5000	630
Çanakkale Çan	1800	320
Kütahya Seyitömer	7100	600
Kütahya Tunçbilek	2450	365
Manisa Soma	8000	1034
Bursa Orhaneli	1500	210
Afşin Elbistan A	18000	1360
Afşin Elbistan B	18000	1440
Sivas Kangal	5400	450
Ankara Çayırhan	4300	620
Total	**80650**	**8079**

economizer, vi) steam drum. These components will below be described below based on Kitto and Stultz [6].

The furnace and evaporator is an enclosed chamber where the coal is combusted to heat the boiler. The **evaporators** provide heat exchange from hot flue gas to water or steam, primarily by convective heat transfer.

Superheater is a part in the boiler designed to remove all moisture from the steam by increasing the temperature of the steam to higher values than its saturation point. **Reheater** is the same but does the same on steam returned from the turbine. In addition, the intermediate-pressure steam has given up some of its energy in expansion through the high-pressure turbine. The operating temperatures of both superheater and reheater are quite high and therefore, tubes used in these parts are heavily alloyed. The position of these tubes, normally in bundles, can be horizontal

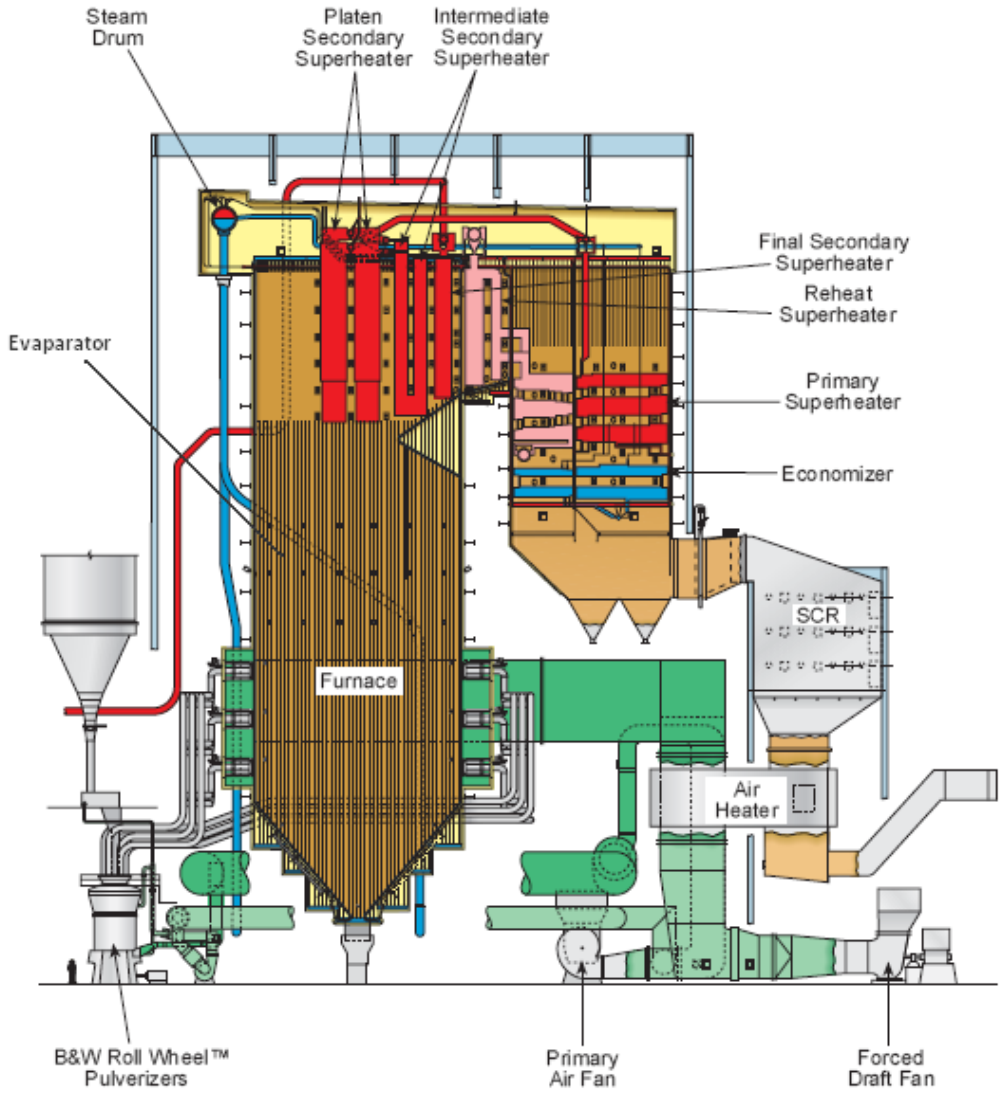

Figure 2.1 Schematic representation of a typical boiler in a coal fired power plant (Kitto and Stultz, 2005) [6]

or vertical in the boiler and the design and location of these tubes are differentiated according to the aimed pressure and temperature of the steam as well as the fuel used.

Economizers are to heat the feed water by extracting the heat from exhaust gases leaving the boiler. Thus, its purpose is to improve the efficiency of the boiler. Tubes in the economizer are very closely spaced so as to provide efficient heat transfer.

Table 2.2 Boiler steam parameters of Çayırhan Thermal Power Plant [7]

Designation	**Parameter**
Maximum continuous superheated steam flow	477t/h
Superheated steam temperature	538^{o}C
Continuous flow of reheated steam	422.6t/h
Reheated steam temperature(in/out)	363.5/538^{o}C
Superheated steam pressure	166 bar
Reheated steam pressure	38.7 bar
Feedwater temperature	250^{o}C
Boiler Efficiency	90%

Table 2.3 Boiler tube materials of Çayırhan Thermal Power Plant [7]

Boiler Parts	**Tube Materials**
Evaporator	15Mo3, 13CrMo44
Sh-1	15Mo3
Sh-2	15Mo3, 13CrMo44
Sh-3	10CrMo910, 13CrMo44
Sh-4	10CrMo910, 13CrMo44
Sh-5	10CrMo910, X20CrMoV121
Rh-1	15Mo3, 13CrMo44, ST35.8
Rh-2	15Mo3, 13CrMo44, 10CrMo910
Eco-1	15Mo3,ST35.8
Eco-2	15Mo3, ST35.8
Drum	Wb36

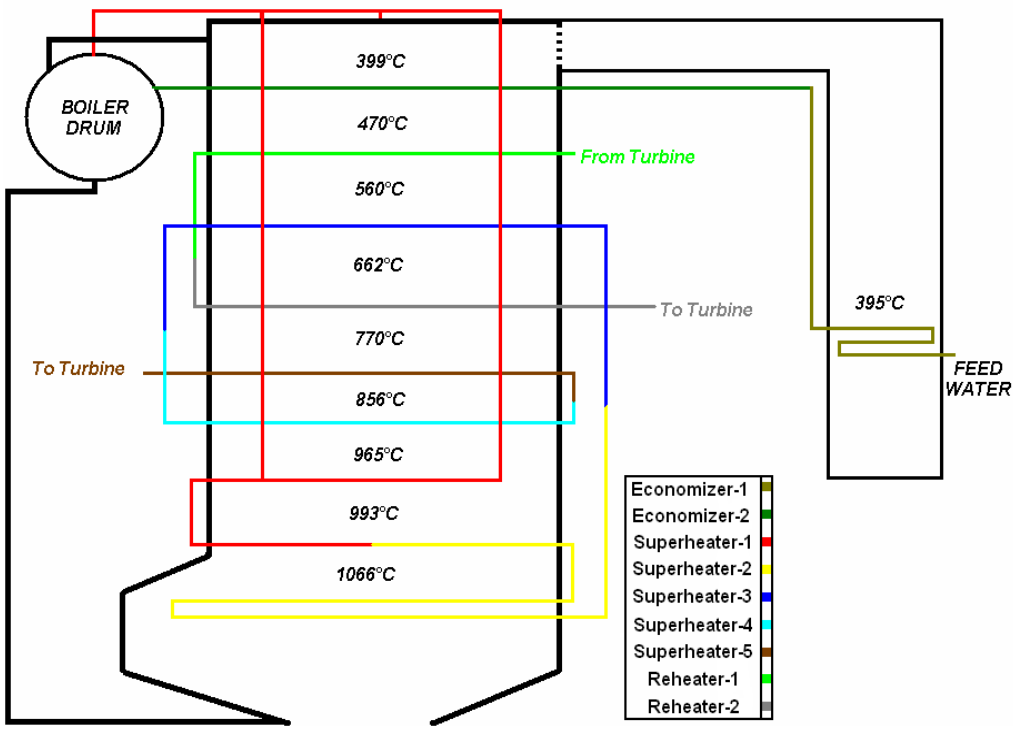

Figure 2.2 Temperature distributions inside the boiler in Çayırhan power plant [7]

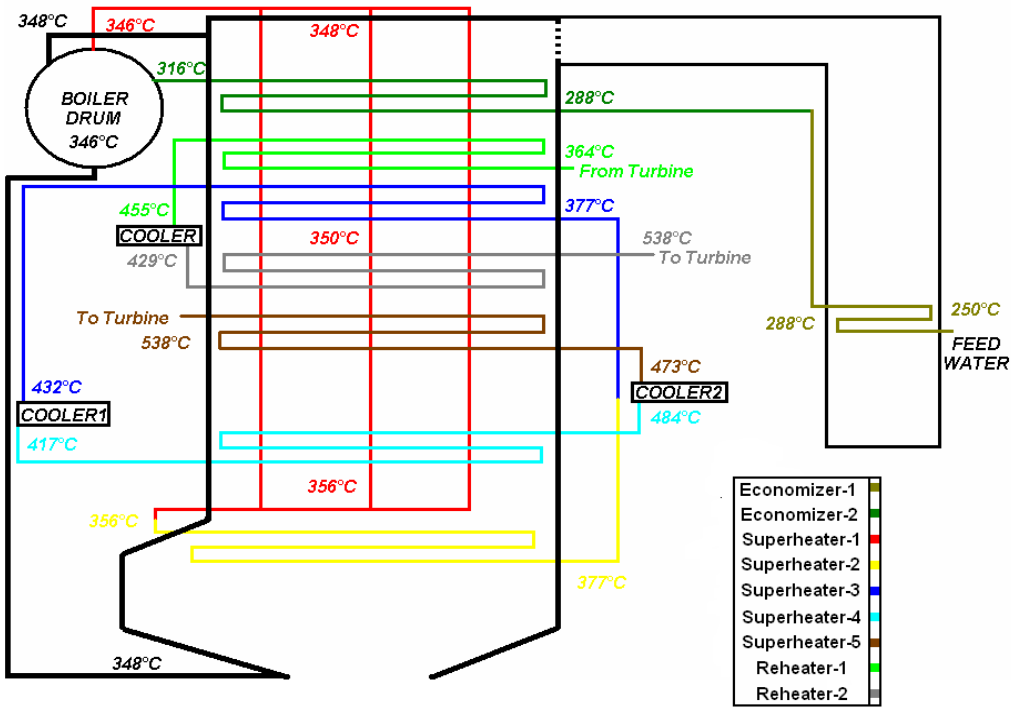

Figure 2.3 Steam temperatures in boiler tubes in Çayırhan power plant [7]

The steam drum is a large cylindrical vessel, located at the top of the boiler. Its purpose is to separate steam from the steam water mixture.

In thermal power plants, boiler tubes are selected from different grades of steel. **Table 2.3** gives the material grades used in different parts of boiler in Çayırhan power plant. This plant operates at 538^{o}C and 166 bar pressure. Temperature distribution inside the boiler is given in **Figure 2.2**. As seen in the figure, the temperature is highest in the burning zone and decreases toward the top and across and down to economizer region. Temperature distribution in the boiler tubes are given in **Figure 2.3**. Here the values again refer to Çayırhan power plant. The temperature in the evaporator tubes is quite low. The temperature at the inlet part of the superheater is 346^{o}C and it increases to 538^{o}C at the outlet. At the reheater, the steam returns from the turbine at 364^{o}C and heated up again to 538^{o}C. In the exit zone of the boiler, the temperature in the economizer ranges from 316^{o}C to 250^{o}C.

2.2 Boiler Tube Failures

According to EPRI 2004 report, the main tube failures observed in coal fired power plants are water-side corrosion, deposit formation and fire-side corrosion, erosion, overheating and fatigue.

2.2.1 Water-side Corrosion

Water-side corrosion refers to inside corrosion of tubes in contact with water or steam. According to the EPRI report [4] water chemistry is an important factor in affecting the internal surface corrosion and operation life of boiler tube materials. The corrosion endurance of the boiler tube is tied on the pH level of the water and the amount of contaminants. Normally, the water is reacted with steel spontaneously at high temperatures and forms a protective layer of magnetite iron oxide (Fe_3O_4)

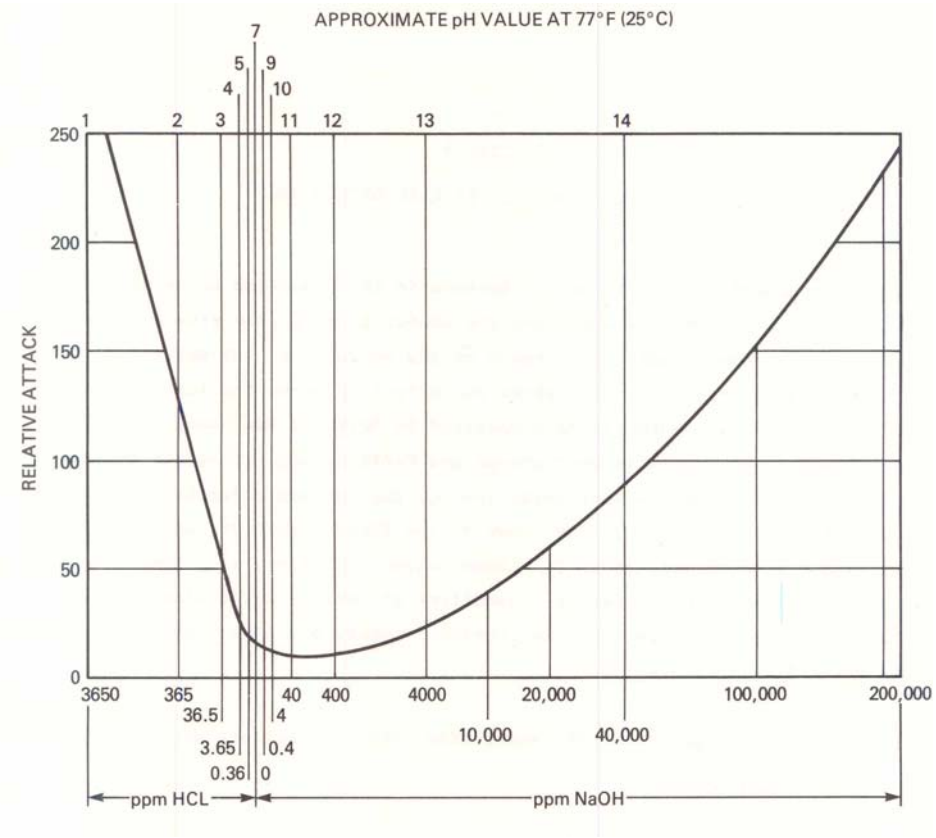

Figure 2.4 Effect of pH on the rate of corrosion of steel by water at 310^{o}C (Grabowski and Klein, 1964) [9]

that ceases the further reaction [8]. **Figure 2.4** is taken from Grabowski and Klein [9] and shows the rate of attack in steel as function of PH value**.** The figure shows that the protective magnetite is unstable and soluble at pH values below 5 and above 12. Normally, in the boiler, water treatment is carried out so as to maintain a moderately alkaline environment so as to prevent the oxide dissolution. EPRI subcategorizes the water–side corrosion into four types which are caustic corrosion, hydrogen damage, pitting (localized corrosion) and stress corrosion cracking. (see Ref. 4)

2.2.2 Deposit Formation and Fire-side Corrosion

Deposit formation refers to fouling of pyrosulfates on the boiler tubes. According to Project Calcium [10], there are two fouling problem in boiler tubes; conventional

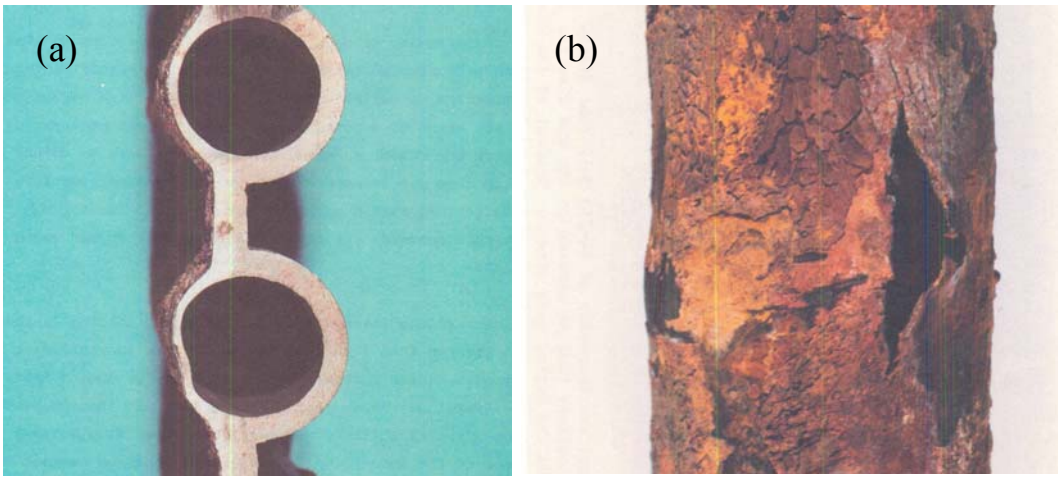

Figure 2.5 a) Waterwall fire-side corrosion, **b)** High temperature coal ash corrosion (EPRI Report, 2004) [4]

high-temperature fouling and low temperature fouling. This distinction refers to the bonding mechanisms of the deposits. In high temperature, the bonding is affected by silicate and iron rich liquid phases. At low temperature the bonding occurs via sulfate formation, such as $CaSO_4$.

The fire-side corrosion refers to corrosion formed on the outer surface of the boiler tubes. The occurrence of fire-side corrosion and the operation life of the boiler tube depend on the fuel ingredients and the metal temperatures [4]. According to EPRI, corrosion failure may be subdivided into subcategories as low temperature corrosion, waterwall fire-side corrosion, high temperature coal ash corrosion. An example of waterwall fire-side corrosion taken from the 2004 EPRI report is given in **Figure 2.5.** This corrosion is reported to occur as a result of incomplete fuel consumption, i.e. at reducing atmosphere which results in the formation of low melting point pyrosulfates (less than 427^{o}C). These molten pyrosulfates may remove the magnetite formed on the surface of the tube and this causes metal disintegration in the outer surface of the tube [11]. High temperature coal ash corrosion is experienced in the superheaters and reheater tubes [12]. This is also known as liquid phase corrosion and is observed when the metal temperature is in the range between 595^{o}C and 705^{o}C.

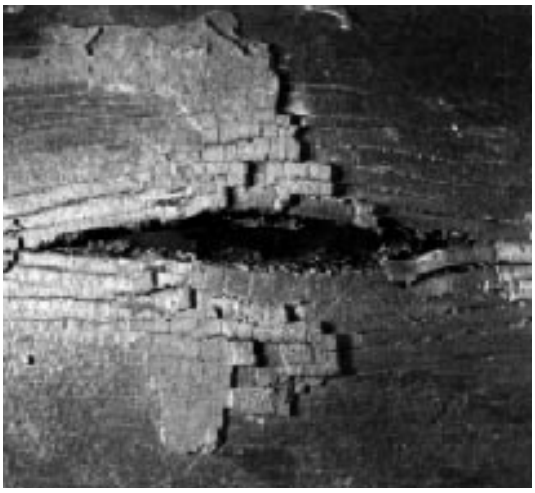

Figure 2.6 Long-term overheating (Babcock & Wilcox Company) [13]

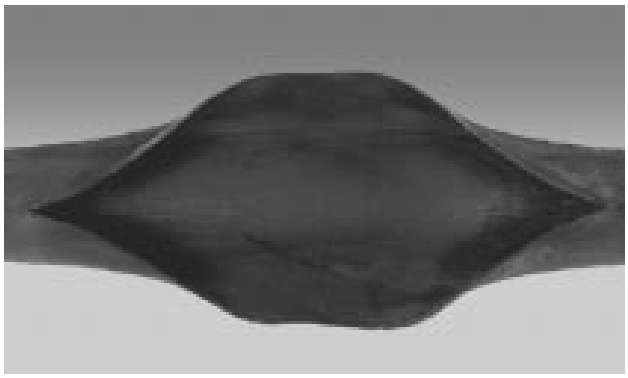

Figure 2.7 Fish mouth opening which arises as a result of short- term overheating **(**Babcock & Wilcox Company**)** [13]

2.2.3 Overheating

Overheating refers to failure of boiler tubes under stress at high temperature. Overheating causes many forced outage because of the boiler tube ruptures. There are two types of overheating: long-term overheating (Creep), short-term overheating.

An example of long-term overheating taken from Babcock and Wilcox [12] is given in **Figure 2.6**. This failure quite common in superheater and reheater tubes is actually a high temperature creep. The timing of failure depends on the level of stress and temperature. The tube may rupture earlier due to high creep rate when the stress and temperature pass over the design values. Long-term overheating failure can be observed also in water wall tubes [13]. In this case, due to scale or deposits that forms at the water-side or due to restricted flow of water/steam, the temperature of the tubes goes up to very high values and the creep failure takes place.

Short-term overheating is the most common failure during the start-up [13]. It is observed when the tube temperature reaches extreme values due to insufficient flow of steam or water. This leads ductile rupture of the tube, the so-called "fish mouth" opening, **Figure 2.7**.

2.2.4 Fatigue

Fatigue refers to failure due to a variety of cyclic stresses on the boiler tubes. During operation of thermal power plants mainly three types of fatigue can be observed: thermal fatigue, mechanical fatigue and corrosion fatigue.

According to EPRI [4], thermal fatigue occurs as a result of rigorous temperature decrease of the tube metal due to water quenching. The main cause of thermal fatigue in economizer tubes is water splashes that occur at the bottom ash hopper and sprays of condensate from the soot blower system. Also rapid and frequent changes in the feed water temperature bring about thermal fatigue resulting in the cracks in the inlet tubes. Cracks propagate through the wall and result in a thick-edged fracture as seen in **Figure 2.8**.

Mechanical fatigue arises from the vibration caused by flue gas flow or sootblowers or due to low frequency high amplitude stresses generated in the boiler. This results

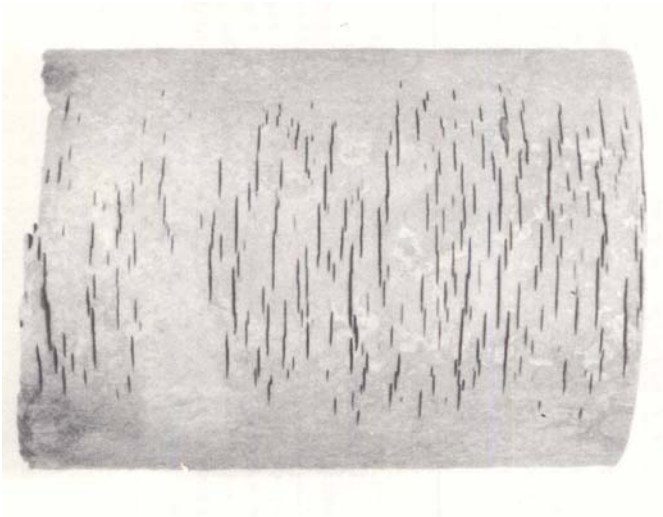

Figure 2.8 Thermal fatigue cracks at the surface of a boiler tube (EPRI Report, 2004) [4]

in thick edged cracks. Corrosion fatigue is combination of thermal fatigue and corrosion [13].

2.2.5 Erosion

Erosion is the removal of material from the tube surface as a result of impacts of ash particles. According to EPRI [4] the amount and velocity of ash particles determine the operating life of boiler tubes since they have serious effect on the amount of erosion. More precisely "For a given concentration of particulate ash in the flue gas, the rate of metal loss is proportional to the impact velocity raised to the power of 3.5." Other parameters controlling the rate of erosion are the angle of impact and the abrasiveness of the ash particles. The economizers, lower furnace sloping tubes, areas adjacent to sootblowers, superheaters, reheaters and cyclone burners are the most common locations where erosion failures are encountered. Erosion of boiler tubes may involve erosion caused by sootblower, by falling slag or by coal particle erosion. But fly ash erosion is most common.

2.3 Fly Ash Erosion Failure

This is the primary erosion failure type encountered in coal fired power plants. It is caused by high velocity fly ash impacting on the boiler tubes. According to EPRI, the particle velocity, the amount of ash particle, as well as the constituents that make up the particles are major factors determining the erosion rate. The velocity of these particles ranges from 15 m/s to 55 m/s. This failure is most common in the economizer due to narrower spacing of the tubes, primary superheater and inlet sections of reheater tubes where the gas flow is non-uniform.

Factors contributing to this failure are several: Blocking of gas passage due to deposit formation results in smaller passages for flue gas and therefore leads to higher velocities. In fact, anything that increases the fly ash velocity contributes to fly ash erosion e.g. misaligned or distorted tubes, or baffles or flow guides which can be misaligned [4].

According to EPRI [4], the fly ash erosion is quite common in economizer. As mentioned above, this is due to close spacing of the tubes. Another factor that contributes to this is the fact that the particles are cooler and more abrasive in this part of the boiler. Initially, the erosion leads to smooth, polished surface, but later on the surface deteriorates by the formation of flow traces and the other formations [12]. It then leads to wall thinning and finally to the tube rupture, **Figure 2.9.**

In order to reduce fly ash erosion, all baffles, collectors; refractories and the like need to be controlled and made sure that they are working properly. If necessary, redesign of boiler parts may be required. It is expected that the decreasing the amount and velocity of fly ash will also lower the damage. Using fuels that would produce less erosive ash may be desirable. Increased flue gas velocity due to high load and excess air results in accelerated failure.

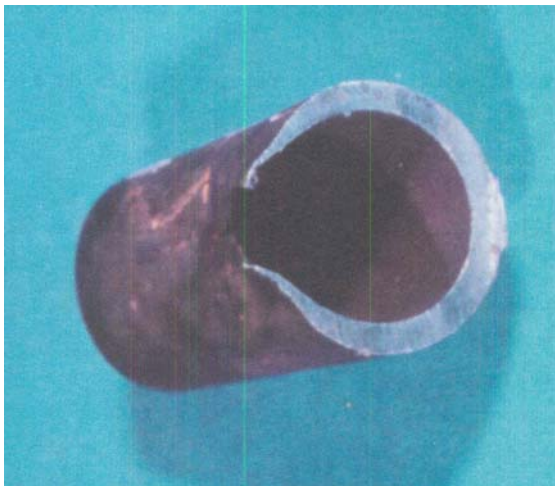

Figure 2.9 Fly ash erosion thinning and failure (EPRI Report, 2004) [4]

The boiler tubes that slag may adversely affect the flue gas velocity and may contribute to the fly ash erosion. Slagging can be diminished by proper fuel additives or soot blowing [11]. Besides, in order to distribute flue gases (and thus fly ash), more evenly, baffle is a reasonable choice. On the other hand, carrying out shielding is impossible where gas flow is horizontal through the tube banks. In this case, slag fences can be used.

It should be pointed out that the potential areas for erosion may be protected by abrasion resistant metal spray coatings.

2.4 Fly Ash in Lignite Fired Power Plants

Erosion failure is closely related to the content of fly ash in the flue gas. Therefore, it is useful to review lignite reserves with respect to their ash content. In Çayırhan power plant the lignite is extracted from the underground mines of Beypazarı Basin, and it has a ash content varying between 30% - 45% [14]. As a result, the plant

Table 2.4 Data for for lignite used in various power plants in Turkey (DEK-TMK) [14]

Power Plant			Lignite			
Name	**Power**	**Annual Lignite Consumption (1000 ton)**	**Calorific (Design) Values (kcal/kg)**	**Ash (%)**	**Moisture (%)**	**Particle size(µm)**
Seyitömer1,2,3	3*150	4,000	1,750±200	35	40	0-200
Seyitömer4	150	1,550	1,650±100	45	40	0-200
Soma A	2*22	270	3500±100	27	22	0-500
Soma B 1,2,3,4	4*165	4,600	2400±100	32	21	0-200
Soma B 5,6	2*165	3,300	1550±100	52	19	0-1000
Çayırhan 1,2	2*150	1,750	2800±200	30	27.5	0-500
Çayırhan 3,4	2*150	2,000	2000±200	45	30	0-200
Orhaneli	210	1,580	2560±%10	30	32	0-1000
Tunçbilek A	2*32,65	490	3600±100	18	22	0-18
Tunçbilek B	2*150	1,950	2170±100	42	24	0-1000
Çan	2*160	1,800	2600±200	32	22	0-1000
Yeniköy 1,2	2*210	3,750	1750±200	29	33	0-600
Kemerköy 1-3	3*210	5,900	1750±200	29	33	0-600
Yatağan 1-3	3*210	4,845	2100±%10	20	34	0-200
Elbistan A 1-4	4*340	18,600	1050±100	17	55	0-1000
Elbistan B 1-4	4*360	17,000	1150±100	19	52	0-1000
Kangal 1-3	2*150,157	5400	1300±100			

consumes 3.75 million tons of lignite and produces 1,350,000 tons of fly ash [15]. The values for other power plants in Turkey can be found in **Table 2.4**.

Chemical make-up as well as particle size of fly ash are also important as erosion depends on the properties and the size of fly ash particles. Fly ash composition of Çayırhan lignite is given in **Table 2.5.** The size is given in **Table 2.6.**

Table 2.5 Fly ash compositions of Çayırhan Power Plant (Şahin, 2005) [15]

Oxide	**Weight%**
SiO_2	50.38
Al_2O_3	14.06
Fe_2O_3	9.90
CaO	13.25
Other Oxides	10.99
Loss on Ignition	0.86

Table 2.6 Fly Ash particle sizes of Çayırhan Power Plants (Şahin,2005) [15]

Mesh size(μm)	**% Passed**
1000	100
500	99.37
250	95.64
200	88.73
106	76.20
90	71.68
45	57.96

2.5 Factors Affecting Erosion Rate

Factors affecting the erosion rate are the concentration of ash particles in flue gas, their impact velocity and impact angle, the properties of the particles themselves and the temperature.

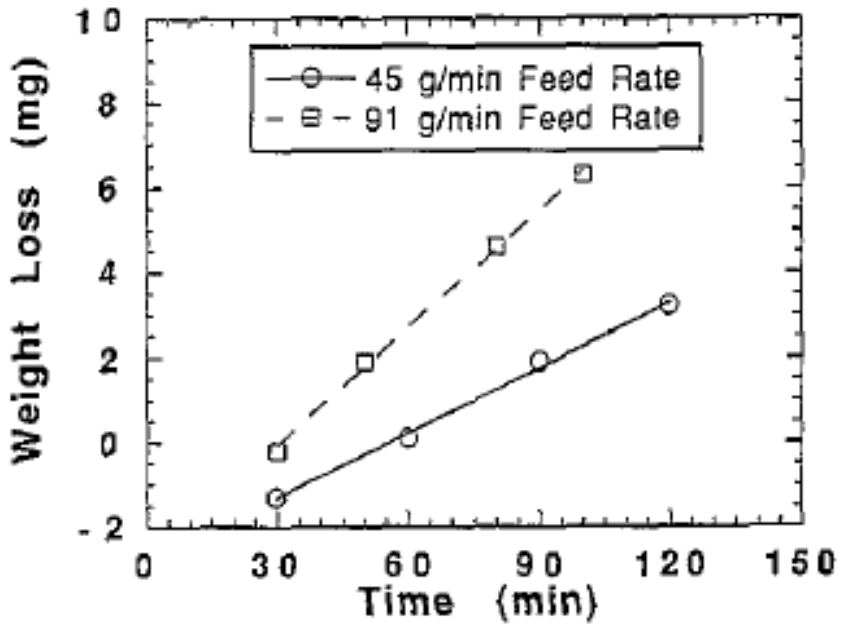

Figure 2.10 Weight loss against time for 1020 steel at 45 and 91 g/min feed rates, 300μm Al_2O_3 erodent, 400°C sample temperature, 40 m/s particle velocity, 90° impingement angle (Lindsley et al., 1994) [16]

The concentration of ash particles is one of the important factors affecting the erosion rate. Lindsley et al. [16] in a special setup have examined the effect of the ash particle concentration using two feed rates. They found that the weight loss increases with increasing feed rate of particles, **Figure 2.10**. The study shows a linear rise of weight loss with time.

Impact velocity of the ash particles was investigated by Zhang et al. [17] and they found that the erosion rate increases with increasing velocity. **Figure 2.11** is taken from Zhang et al. which shows that the relationship is not linear. As seen in the figure, the erosion rate increases more rapidly at higher values of the impact velocities. Zhang at al. explain this based on the argument that impact energy is proportional to square of the velocity. The effect of the impact velocity was also studied by Suckling and Allen [18] who has reported similar results, see **Table 2.7**.

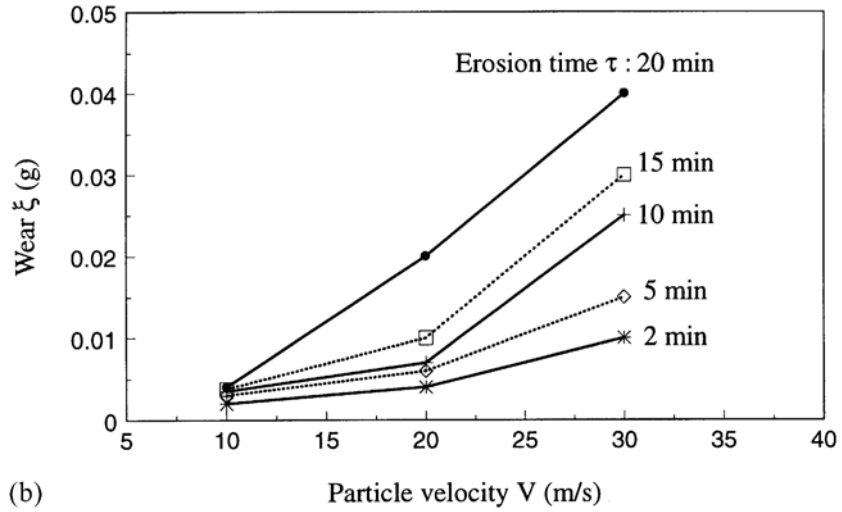

Figure 2.11 Effect of particle velocity on erosion wears (The erosion conditions are c=185.6 g/m^3, α=90^o) (Zhang et al., 2001) [17]

Table 2.7 Erosion wear rates for three set temperatures, the four velocity value were tested. (Suckling and Allen, 1997) [18]

Velocity	52 m s^{-1} Erosion rate cm^3/9×10^{-5}	41 m s^{-1} Erosion rate cm^3/9×10^{-5}	33 m s^{-1} Erosion rate cm^3/9×10^{-5}	24 m s^{-1}	
				Erosion rate cm^3/9×10^{-5}	exponent n
100 °C	4.0	2.4	1.3	0.8	2.12
300 °C	4.5	2.7	1.5	1.0	1.98
450 °C	6.2	3.7	2.1	1.5	1.87

Zhang et al. in their study also looked at the effect of the impact angle on the erosion. Working on a ductile tube specimen (AISI 1015), they found that the erosion varied as a function of impact angle. Using SEM (Scanning Electron Microscope) they observed that at rubbing and scratching up to 10^o of impact angle. At 20^o the effect was in the form of cutting. At 30^o, cracking, at 60^o extrusion and finally at 90^o, they observed sputtering. The effect on erosion, **Figure 2.12**, was such that the rate was highest at impact angle of 20^o - 30^o.

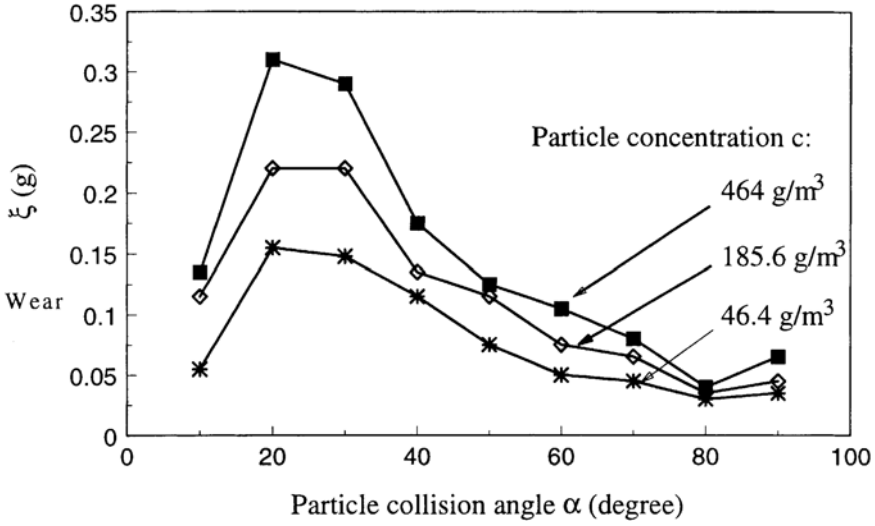

Figure 2.12 Variation of material removal with particle collision angle (The erosion conditions are V=20 m/s, t=52 min.) [21] (Zhang et al., 2001) [17]

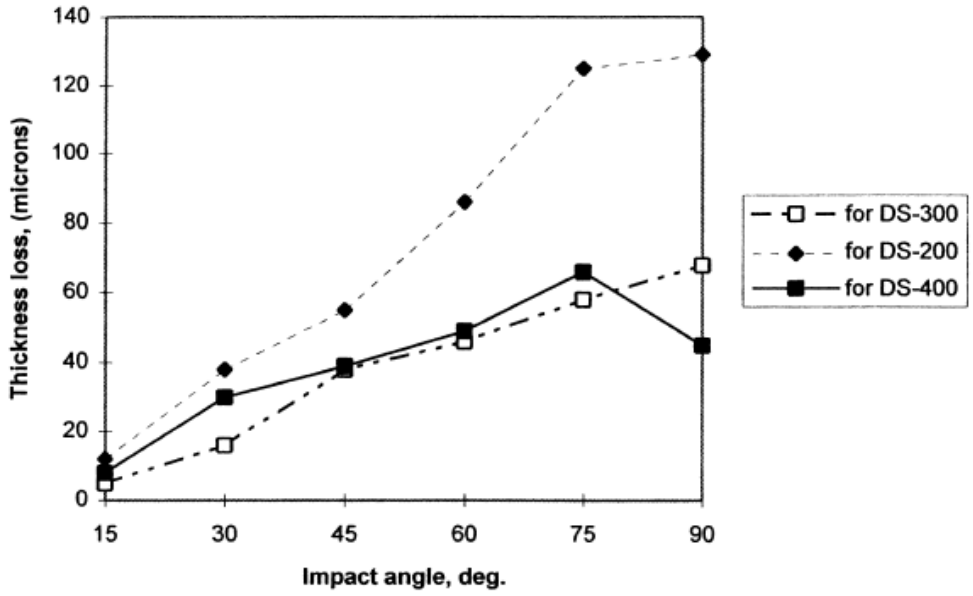

Figure 2.13 Erosion thickness loss vs. impact angle for three coatings eroded by bed ash (under V=60 m/s, T=300°C, t=5 hours, 375 g) (DS-200=Cr_3C_2–NiCr, DS-300=Cr_3Cr_2/TiC–NiCrMo, DS-400=NiAl–40Al_2O_3) (Wang and Lee, 1999) [19]

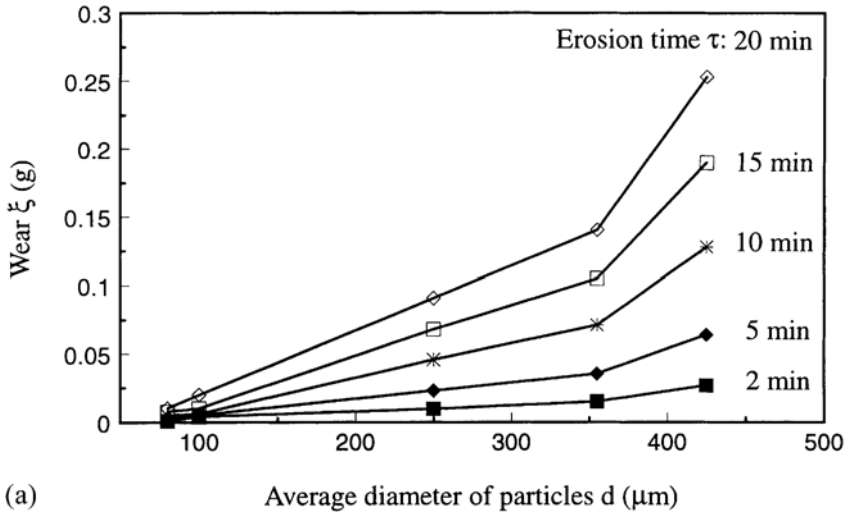

Figure 2.14 Effect of particle size on erosion wear at various erosion time (The erosion conditions are V=20 m/s, c=185.6 g/m^3, α=90^o) [21]

The effect of impact angle depends on material. Wang and Lee [19] have studied the effect of impact angle on the erosion of NiAl-40Al_2O_3 (DS400) coating and found that the erosion increases with increasing impact angle, **Figure 2.13**.

Effect of particle size on erosion has been studied by Zhang et al. [17]. **Figure 2.14** is taken from their study and shows that the erosion increases with increasing particle size. Desale et al. [20] investigated three different erodent material; quarts, alumina and silicon carbide. The sample was AISI 304L steel. They examined the effect of particle shape, defined in terms of a shape factor, on erosion. The properties of the particle samples used in test are given in **Table 2.8**. Besides they observed also the effect of the erodent density on the erosion rate. The study has shown that increasing shape factor leads to erosion rate decrement and but increasing density affects the erosion rate positively. This can be derived from the surface roughness comparisons of the specimens. The surface roughness comparisons of two specimens with different particles at different angles for shallow and normal angle values are indicated in **Table 2.9**.

Suckling and Allen have studied the erosion of 1Cr1/2Mo steel from 20^{o}C to 600^{o}C. They found that the erosive wear increases with increasing temperature, **Figure 2.15**.

Table 2.8 Physical properties of erodent materials (Desale et al., 2006) [20]

Erodent particles	Hardness (Hv)	Density (kg m^{-3})	Modified shape factor	Particle shape
Quarts	1100	2650	0.7007	Blocky
Alumina	1800	3940	0.3425	Angular
Silicon carbide	2500	3220	0.4425	Angular

Table 2.9 Worn out specimen surface morphology due to impact of different solid particles (Desale et al., 2006) [20]

Erodent	Orientation angle (°)	Average surface roughness ($\times 10^{-3}$ μm)	Distance between peak-to-valley (μm)
AA6063			
Quartz	15	566.66	6.85
SiC	15	732.9	8.67
Alumina	15	810.23	11.75
Quartz	90	584.08	7.42
SiC	90	707.93	8.35
Alumina	90	927.23	11.66
AISI 304L steel			
Quartz	15	404.23	6.51
SiC	15	496.73	7.86
Alumina	15	619.10	9.07
Quartz	90	399.78	5.76
SiC	90	494.12	6.81
Alumina	90	604.77	11.09

Tylczak et al. [21] in a similar study examined the erosion of a number of materials; T-22 type (2.25 Cr 1 Mo steel), 304SS, 310SS and Incoloy 800 from room temperature to 800^{o}C. They concluded that the material loss increases at high temperatures, **Table 2.10**.

The material properties are also influential in affecting the erosion rate. The material composition, the heat treatment history and surface hardness are all relevant in the erosion phenomena. Hayashia et al. [22] investigated the effect of Cr concentration in steel on erosion resistance. They observed that increasing Cr content of steel reduces the material loss in erosion. This effect was particularly pronounced in low concentrations which continued up to 10% Cr.

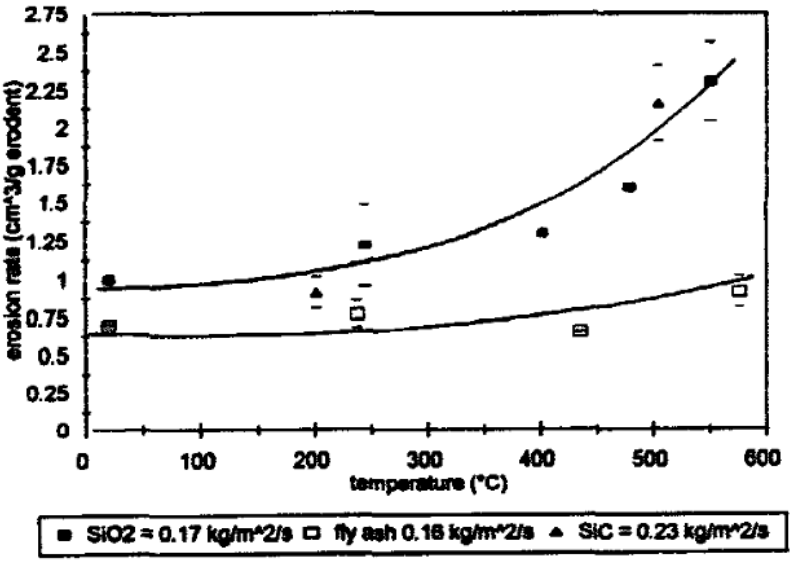

Figure 2.15 Graph showing differences in particle erosivities of SiO_2, SiC and fly ash at a constant particle velocity V = 24±2 m/s and a particle flux between 0.16 and 0.23 kg/m^2s.(Suckling and Allen, 1997) [18]

Table 2.10 Erosion loss for various conditions, in mmpy (Tylczak et al., 2003) [21]

Conditions			Alloy, loss in mmpy			
Temp, deg C	Atmosphere	Speed, m/sec	2 ¼ Cr 1 Mo	304 SS	310 SS	Incoloy 800
Room	Air	20	0.5	0.6	0.6	0.5
500	Air	20	12.7	0.7	0.5	0.8
500	Gasifier	20	20.9	8.4	22.4	7.6
500	Gasifier	30	30.2	16.7	20.9	4.5
600	Gasifier	20	24.5	11.7	9.2	7.0

Sagayaraj et al. [23] have looked at the erosion of economizer tube (SA 210 GrA1) both in normalized and annealed condition The experiments showed that the erosion rate of the normalized carbon steel is higher than that of the annealed carbon steel.

Wang and Lee [19] have investigated the resistance of various coatings and AISI1018 steel against erosion. They evaluated NiAl-40Al_2O_3 and three different intermetallic-ceramic coating applied by HVOF on AISI 1018, **Table 2.12**. They found that NiAl-40Al_2O_3 coating possesses the highest erosion resistance among other coatings.

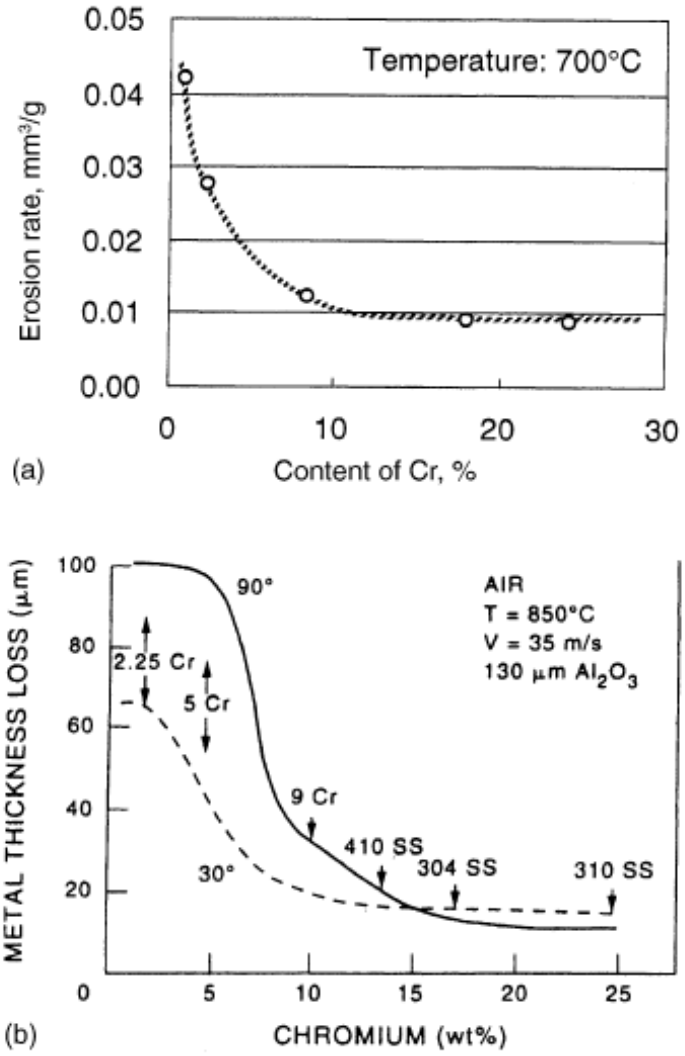

Figure 2.16 Relationship between content of Cr in steels and erosion rate: a) data obtained by the centrifugal apparatus (particle: SiO_2 (average diameter: 23 μm), particle impingement angle: 30^o, temperature of test piece: 700^oC) and b)data obtained by blast type apparatus (Hayashia et al., 2003) [22]

Table 2.11 Target coating Materials (Wang and Lee, 1999) [19]

Coating	Process	Nominal Composition	Thickness (μm)	Hardness (HV)	Porosity (%)
NiAl–40Al_2O_3 (DS-400)	HVOF	30Al_2O_3/70NiAl	370–420	411	<2
Cr_3C_2/TiC–NiCrMo (DS-300)	HVOF	75 Cr_3C_2/TiC–25NiCrMoAl	300–350	670–720	<2
Cr_3C_2–NiCr (DS-200)	HVOF	75 Cr_3C_2–25NiCr	225–275	620–690	<2
FeCrSiB (Armacor M)	arc-spray	Fe25Cr3B2Si	260–300	650–740	4–6

Table 2.12 Thickness loss of target materials tested under condition (T=300°C, V=60m/s, 375g bed ash) (Wang and Lee,1999) [19]

Target materials	Thickness loss (μm)	
	at $\alpha = 30°$	at $\alpha = 90°$
1018 steel	308	231
NiAl–40Al_2O_3	30	45
Cr_3C_2 /TiC–NiCrMo	16	68
Cr_3C_2 –NiCr	40	138
FeCrSiB	91	435[a]

2.6 Test Setups for Erosion of Boiler Tubes

Studies reported above concerning factors affecting the erosion rate have mostly been carried out in experimental setups that have been developed for the purpose. One such setup is that of Moumakwa and Marcus [24]. Schematic representation of this setup is given in **Figure 2.17.** The setup operates by injecting erodent particles with a gas stream to impact onto the target specimen placed in an enclosed chamber. In this system, by changing the pressure of the carrier gas (compressed air) the velocity of erosive particles can be adjusted. The feed rate of erosive particles is controlled by the venturi educator which draws the particles from the revolving table whose rotation speed is controlled by an electric motor. The sample was mounted on a variable angled block so that the impact angle can be changed at ease. Particles used in this setup were 125-180 μm silica.

The setup allows the study of effects of various parameters on erosion but the tests were limited to room temperature.

Zhang et al. [21] have described an erosion apparatus that can be used with tubular samples. The setup, given in **Figure 2.18,** allows the flow rates of particles up to 30 m/s by changing the air pressure. Erodent particles were directed by a nozzle to the surface of specimen, the axis of the nozzle always aligned with the diameter axis of the tubular sample. The nozzle angle with respect to the longitudinal axis of the tube

Figure 2.17 Schematic representation of the room temperature gas-blast erosion

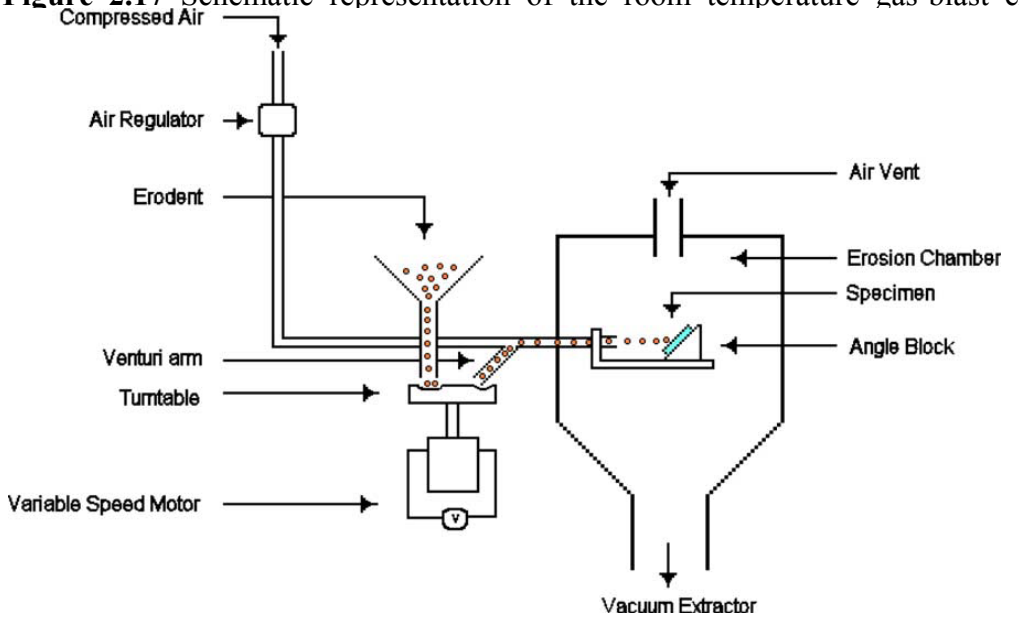

apparatus (Moumakwa and Marcus, 2005) [28]

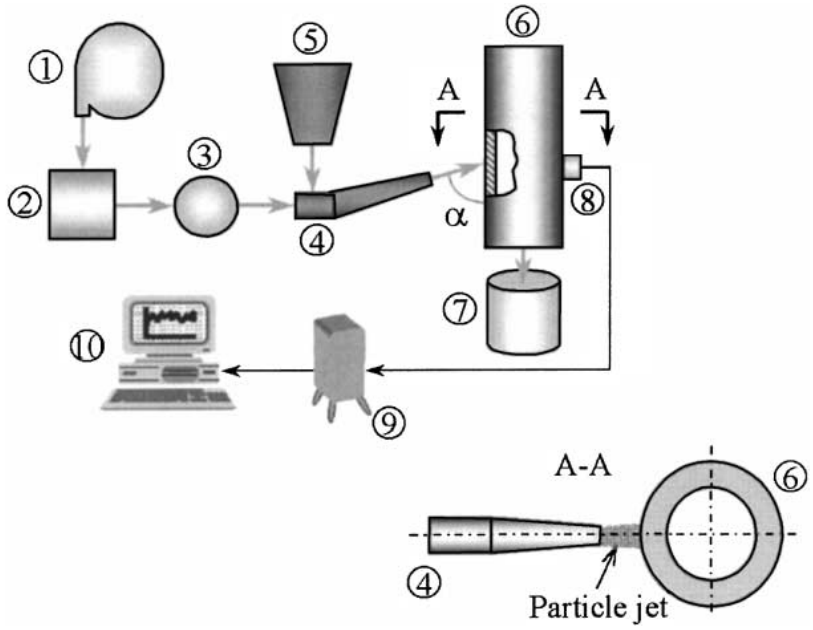

Figure 2.18 Acoustic Emission Test Setup (1) the air compressor, (2) the pressure regulator, (3) the flow meter, (4) the nozzle (16mm in diameter), (5) the particle container, (6) the tube specimen (63mm in diameter), (7) the particle collector, (8) the acoustic sensor, (9) the amplifier and (10) the computer. (Zhang et al., 2001) [21]

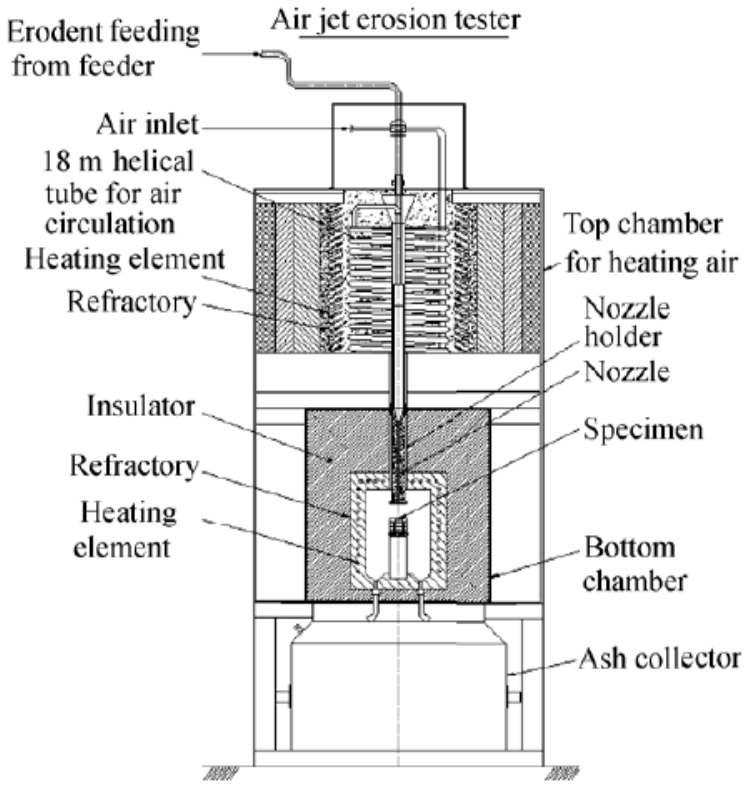

Figure 2.19 Erosion test rig (Sagayaraj et al., 2008) [23]

was adjustable from 0 to 90^{o}. By this way the impact angle, α, could be controlled. The erosion severity was measured by observing the material loss.

Sagayaraj et al. [23] have described a setup that allows high temperature testing. The setup, given in **Figure 2.19,** composed of a furnace and a particle feeding system based on compressor.

Suckling and Allen [18] have described an erosion setup that can be used for high temperature tests. Schematic representation of this setup is given in **Figure 2.20**. Heating was achieved by LPG flame. In this system angled block is used as sample holder.

A more comprehensive setup, is that of Lindsley et al. [16], **Figure 2.21.** This allows testing of samples from 25^{o}C to 1000^{o}C. The impact angle can be adjusted from 0^{o}

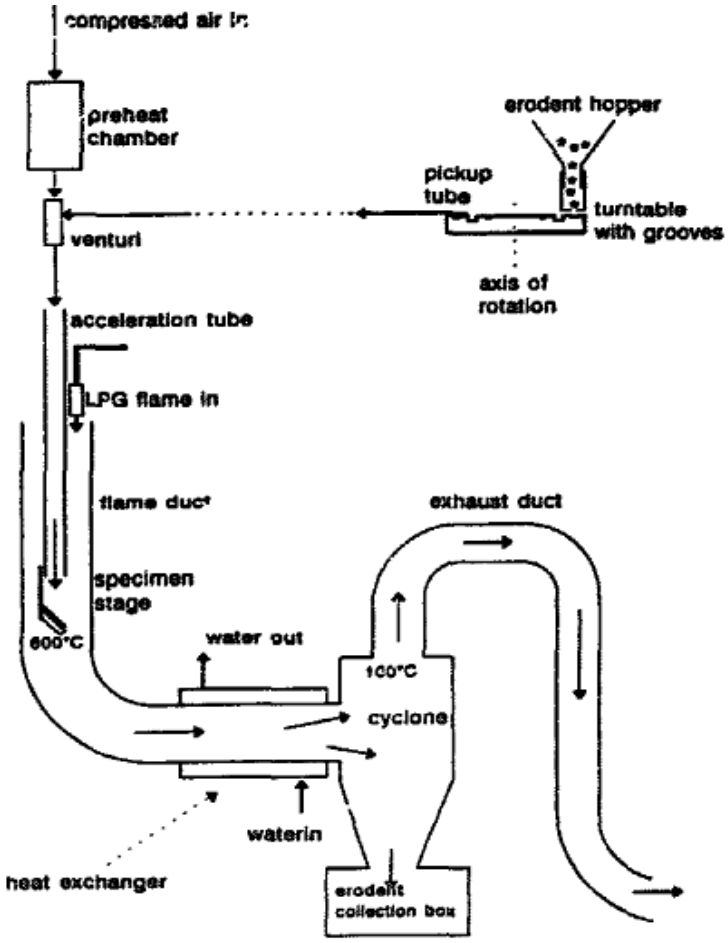

Figure 2.20 Diagram of high temperature erosion apparatus used to simulate the required boiler conditions. (Suckling and Allen, 1997) [18]

and 90^{o}. The velocity of particles (Al_2O_3) could be increased up to 85 m/s. The feed rates of particles are adjusted with a screw feeder driven by variable speed motor. The sample is placed inside a furnace which could be heated up to 1200^{o}C. The air carrying the particles is preheated before entering the furnace. The particles can be accelerated in a SiC tube before they hit the surface of the sample. The impact velocity of the particles are measured with a TSI laser Doppler velocimeter that provides direct measurement of the particle velocity without disturbing the particle flow, upon exiting the acceleration tube. The powder and gas mixture which come

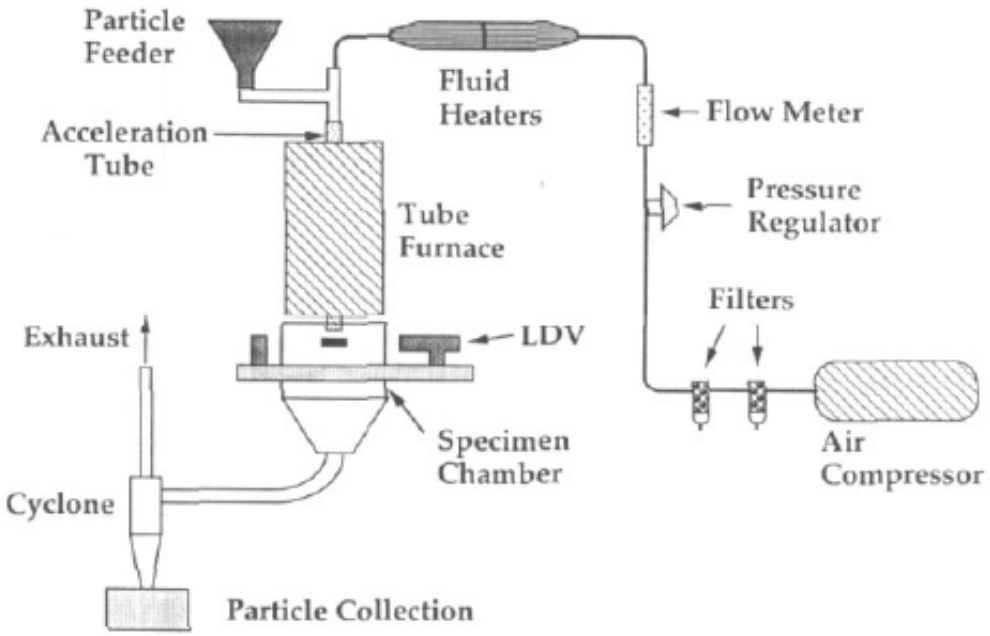

Figure 2.21 High-temperature erosion apparatus schematic (Lindsley et al., 1994) [16]

out trough the system are segregated with the help of a cyclone. Besides, SO_2 gas is able to be sent to the system to simulate corrosion mechanism in this setup.

Tylzcak et al. [21] designed a test apparatus, named as the Hostile Atmosphere Erosion Test Apparatus (HEAT Apparatus), that is quite different from the conventional setups, **Figure 2.22**. This system is working in a closed furnace, isolated by heat shields. The sample is inside the furnace connected to a shaft, inserted vertically through a lid. The shaft and hence the sample is rotating by a variable speed motor. Erosive particles (SiO_2) are fed by a screw feeder into a long abrasive feed tube which injects the powders onto the sample.

Hayashia et al. [21] have described a setup that allows a number of samples to be tested at the same time. Schematic representation of this setup is given in **Figure 2.23**. In this apparatus erosive particles were fed into a central hopper to which a nozzle is attached. The particles are delivered onto the samples placed at the periphery with a high speed as a result of a centrifugal force of a rotating hopper. The

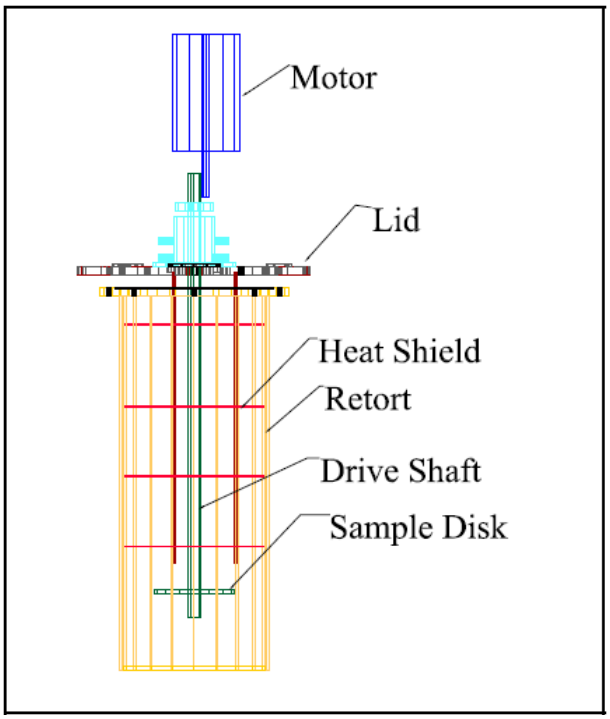

Figure 2.22 The diagram of the HEAT Apparatus (Tylzcak et al., 2003) [21]

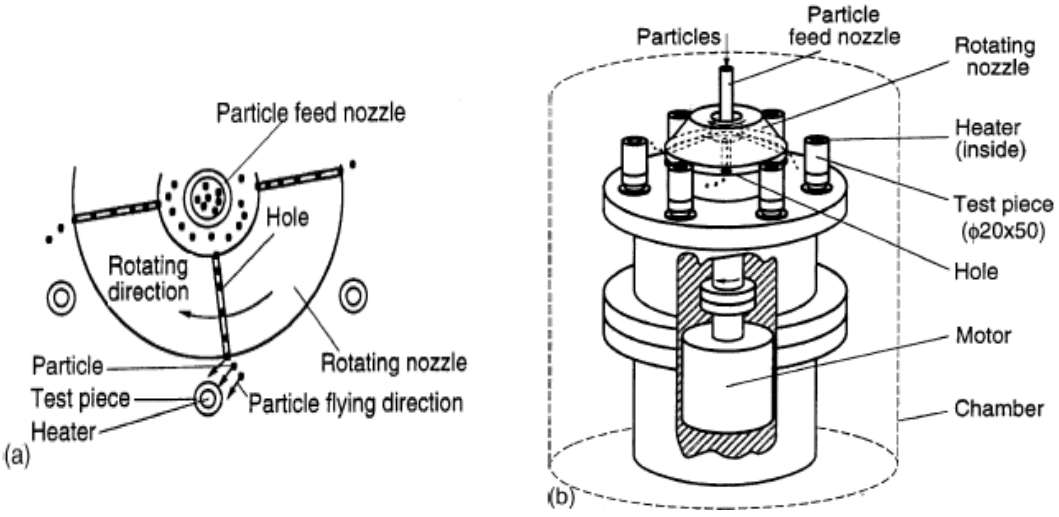

Figure 2.23 Main structure of the centrifugal high temperature erosion apparatus: a) principal of centrifugal erosion apparatus and b) structure of the main part of apparatus (Hayashia et al, 2003) [26]

test could be conducted at different temperatures. A total of 6 samples could be tested simultaneously in this setup.

CHAPTER 3

EXPERIMENTAL SETUP

Apparatus constructed in this thesis aims primarily for erosion tests of boiler tubes. In addition, the apparatus can also be used for creep testing as well as for corrosion testing of boiler tubes. The design of this setup was based on the preliminary study carried out by a group of 4^{th} year undergraduate students (T7) of Metallurgical and Materials Department of Middle East Technical University in the year 2007 [25].

Test apparatus was designed to simulate operating conditions in the boiler of thermal power plants especially in the economizer zone. The setup consists of three components, **Figure 3.1**. These are i) a unit for sample loading, ii) a unit for blowing the abrasive particles, and iii) a heating system to control and monitor the temperature of testing.

3.1. Sample Loading System

A schematic drawing of a sample loading system is given in **Figure 3.2**. The system comprises a tubular mill (1) housed in place with the use of two bearings (2). Further below, there is an identical mill (3) of a short length fixed axially in place and centered in a similar bearing (4). Sample (5) is connected axially to these mills via a pin coupling (6).

The sample is loaded with a spring system. The spring (7) can be compressed with a help of a gear-nut (8) rotated with a gear connected to a motor placed on a horizontal plane (not shown). With the sample in its place; when the nut is driven down, it compresses the spring applying tensile forces to the mill and hence to the sample.

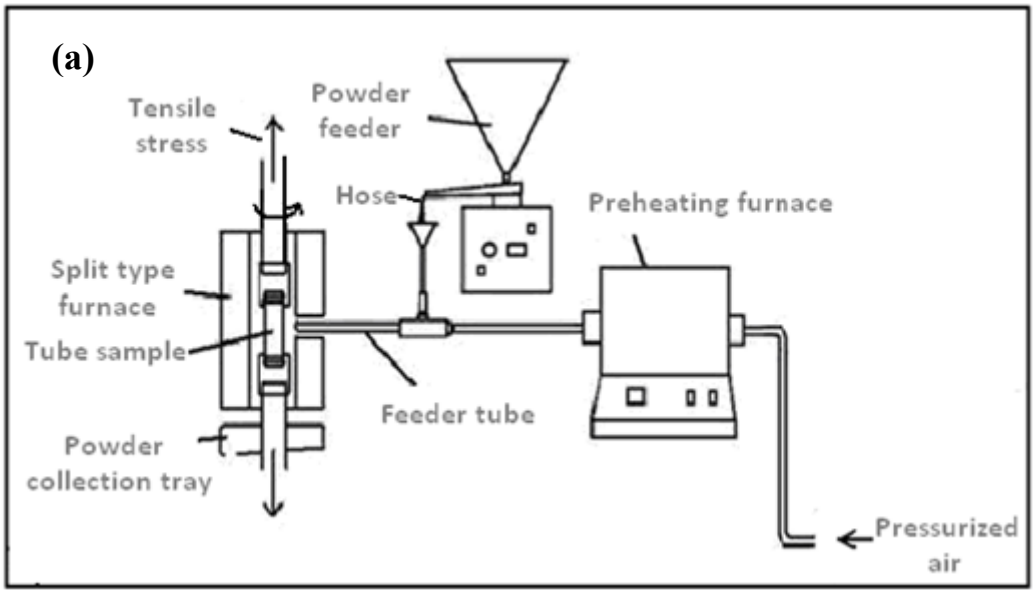

Figure 3.1 a) Schematic representation of test setup simulating operating condition of the thermal power plant boiler tubes **b)** Photograph of the test apparatus

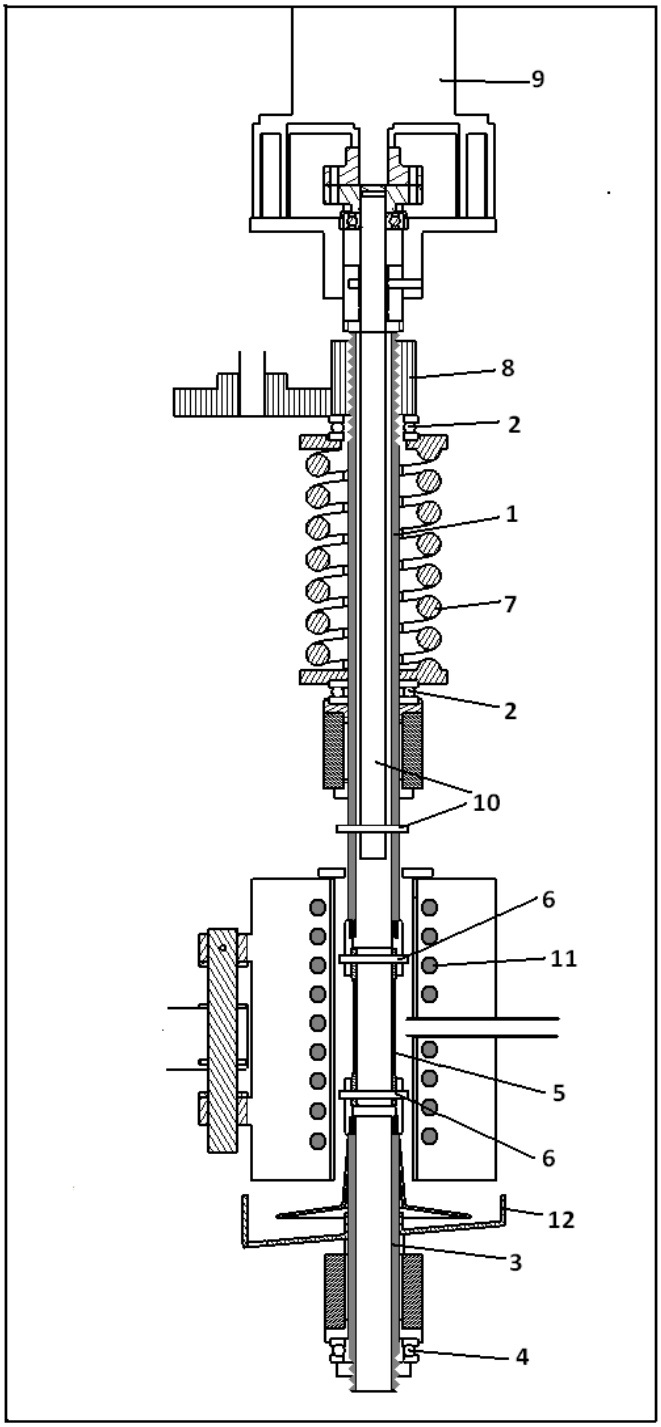

Figure 3.2 Sample loading system in the setup, see text for details. 1. Tubular upper connector mill, 2.Axial bearings, 3. Tubular lower connector mill, 4.Axial bearing, 5.Sample, 6.Connecting pins (sample), 7.Helical compression spring, 8.Gear, 9.Motor with a reduction gear, 10. central mill with a connection pin , 11.Heating elements, 12.Tray for powder diversion.

Table 3.1 Stress values of Çayırhan Thermal Power Plant Boiler Tubes (T7 Report, 2007) [25]

	20CrMoV121	**14CrMo44**	**15Mo3**	**10CrMo910**	**St35.8**
R inner (mm)	15.95	17.25	15.15	15.15	24.7
R outer (mm)	22.25	22.25	22.25	22.25	28.7
Yield strength (MPa)	250 (at550oC)	190 (at480oC)	163 (at460oC)	185 (at500oC)	110 (400oC)
Thickness (mm)	6.3	5	7.1	7.1	4
Pressure (MPa)	16.6	16.6	16.6	16.6	5.6
Longitudinal Stress (MPa)	17.5	25	14.3	14.3	20.09
Hoop Stress (MPa)	41.4	56.8	34.7	34.7	40.2

3.1.1 Selection of Spring

The loading system as described above allows the use of samples in the form of tubes with a minimum of sample preparation. The sample preparation consists of machining of the central portion of the tube and drilling of two holes at both ends of the sample.

In this design, since loading is effected by spring, the selection of the spring is quite critical. To be able to decide about the characteristics of the spring first it is necessary to determine the level of stresses generated in the boiler tubes.

Boiler tube data of Çayırhan power plant are given in **Table 3.1.** Based on this data stresses generated in the tubes have been calculated and are included in the table. By looking at these values, it is seen that the hoop stress, which is twice the longitudinal stress has a maximum value of approx. 57 MPa. This value is nearly 1/3.5 of the yield stress of the material in question. See Table 3.1. Even though system stress in the tubes are that of plane stress, the loading system as described above apply uni-axial stress. Considering that the maximum value was 57 MPa the uni-axial loading with 100 MPa was considered to be sufficient for the current purposes.

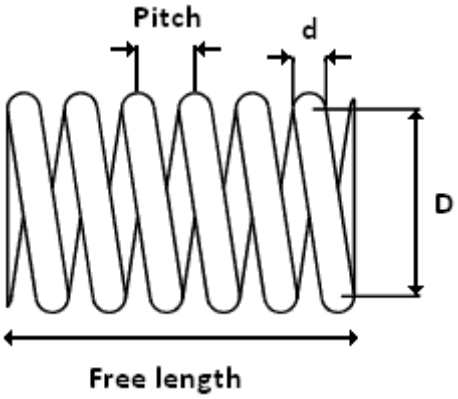

Figure 3.3 Helical spring

To be able to select the spring, it is now necessary to decide about the sample dimension. As seen in Table 3.1 the tube diameter varies from 44.5 mm to 57.4 mm. The wall thickness of boiler tubes varies from 4 mm to 7.1 mm. Thus, the cross-sectional areas of the tubes have a value in between $6.71 \times 10^{-4} m^2$-$8.34 \times 10^{-4} m^2$. To generate uni-axial stress of 100 MPa it is necessary to apply a force of 67,100 N to 83,400 N. This force is quite large and so as to reduce the level of required force the cross-section of the sample was reduced by machining the tube down to approx. 2mm wall thickness. With tube diameter of 35 mm and the wall thickness of 2mm 100 MPa stress corresponds to the application of tensile forces of approx. 20,000 N.

Figure 3.3 shows a helical spring. Here d is the diameter of the spring material, and D is the mean diameter of the coil. Force, F generated axially by the coil is given by [26]

$$F = k.\Delta \qquad (4.1)$$

Where

$$k = \frac{G.d^4}{8.n.D^3}$$

Here k is the spring constant, Δ is the deflection, G is the shear modulus of the material, n is the number of active coils.

Table 3.2 Compression spring types and their properties [27]

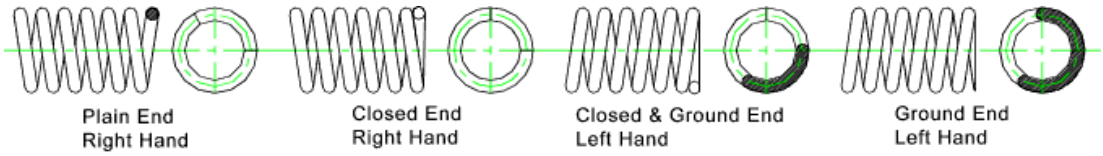

Term	Plain	Plain and Ground	Closed	Closed and Ground
End Coils (n_e)	**0**	1	2	2
Total Coils (n_t)	**n**	n+1	n+2	n+2
Free Length (L_0)	**pn+d**	p(n+1)	pn +3d	pn +2d
Solid Length (L_s)	**d(n_t +1)**	dn_t	d(n_t +1	dn_t
Pitch(p)	**(L_0-d)/n**	L_0/(n +1)	(L_0-3d)/n	(L_0-2d)/n

The number of active coils is equal to the total number of coils n_t minus the number of end coils n_e that do not help carry the load, [26]

$$n = n_t - n_e \qquad (4.2)$$

There are several alternatives for spring selection, **Table 3.2**. Of these closed and ground type helical spring is particularly suitable since they have flat ends.

As for the spring material, AISI 9250 (ASTM A-401) is quite common known also as Chrome silicon steel. The properties of this steel are given in **Table 3.3**.

Following the above consideration, helical spring of mean diameter (D) of 123mm was selected. The other parameters of the spring are given in **Table3.4**. The spring has a torsional modulus of 79.3GPa. Inserting the relevant dimensional parameters the spring has a spring constant of k=346,000N/m. Thus, up on deflection of 85% maximum deflection recommended for such springs, this generates a tensile force of approx. 30,000N. This value is safely above the targeted value of tensile stress which was 20,000N.

Table 3.3 Properties of AISI 9250 (ASTM A-401) steel [28]

Chemical composition	C(0.51-0.59%),Cr(0.60-0.80%),Si(1.20-1.60)
Tensile Strength	1600-2050MPa
Elastic Modulus	205Gpa
Torsional Modulus	79.3GPa
Rockwell Hardness (Rc)	48-55
Method of Manufacture	Cold drawn and heat treated before fabrication. Used shock loads and moderately elevated temperature

Table 3.4 Dimensions of the helical spring selected for the apparatus

Number of active coils	6
Mean diameter (D)	123 mm
Coil diameter (d)	25 mm
Pitch length	41.3 mm
Space between coils	16.3 mm
Free length	248mm

Table 3.5 The properties of the helical spring

Spring constant (k)	346 N/mm
Max. theoretical deflection (85% of space between coils) Δ_{max}	83.3 mm
Max. force generated by the spring	28,821 N

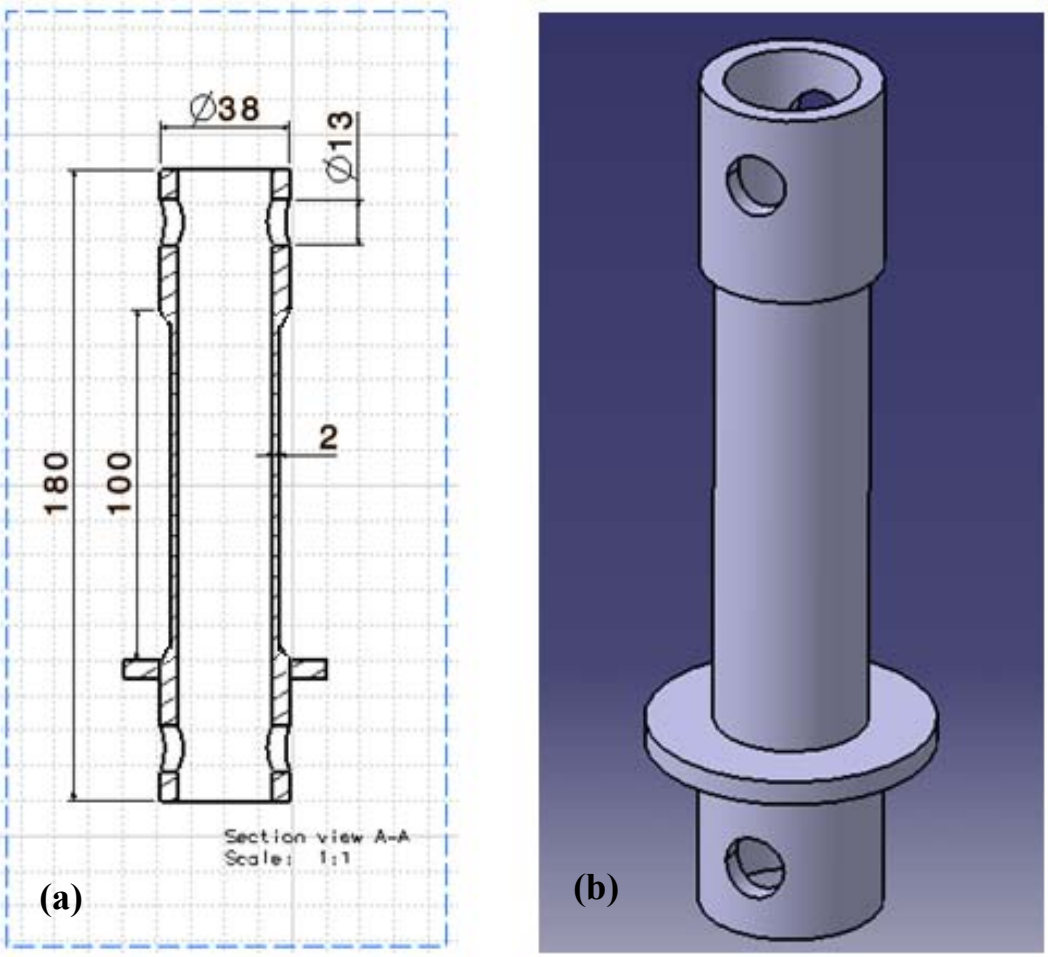

Figure 3.4 Test piece used in the setup. **a)** Section view **b)** 3-D view

The above calculations were checked by testing the selected spring by compression loadings. Force versus deflection values are reported in **Table 3.5**.

3.1.2 Sample Preparation

It is highly desirable to test the samples directly cut from the tubes. However, the cross-sectional area of the tubes are quite large and to be able to generate a comparable stresses, a very high forces would be needed. As a result, samples have been machined to reduce their cross-sectional area. Figure4.5 shows a schematic

Table 3.6 Deflection tests of the helical spring

Load applied	**Deflection**
500kg	15mm
1000kg	30mm
2000kg	60mm
2250kg	67mm

representation of the sample used for testing. As seen in the figure test piece has two pin holes which are used for the connectiom of the test piece to main test shaft. Here the collar seen close to the lower end of the sample is firm fitted to the sample diverting the abrasive particles away from the pin coupling.

3.1.3 Electric Motors and Auxiliary Units of the Loading system

To load the helical spring, a horizontal reduction gear motor, with a 0.55 kW power and 1033 Nm torque capacity, is selected. The rotation speed of this unit is 4.7 rpm. This motor-gear was placed onto a platform supported by a column, shown in **Figure 3.5**. To generate force, this unit is engaged to spring gear on the tubular mill. The diameter ratio is such that spring gear has a speed of 7.83 rpm. The spring-gear as a result moves downward on the tubular mill (1) compressing the spring (see Figure 3.2). Ones the required level of force is reached the motor-gear was disengaged. Since the tubular mill is free to move vertically on the inner mill, the spring exerts tensile force on the sample.

Calculations show that to be able to compress the spring to apply force of 20,000 N it is necessary to apply a torque of approx. 300 Nm on spring gear. Since the reduction gear motor has a torque of 1033 Nm this is more than sufficient to compress the spring.

Figure 3.5 Photograph of reduction gear motors and the spring.

The tubular mill was manufactured from specimen AISI 316 stainless steel [29]. The central mill which rotates the sample together with the tubular mill was again AISI 316 stainless steel.

3.2 Heating System

For heating system a split type furnace is used. This unit was connected to platform carrying the reduction gear motor. The furnace refractory (Al_2O_3-SiO_2) with

Figure 4.5 Furnace refractory elements with embedded Khantal resistors

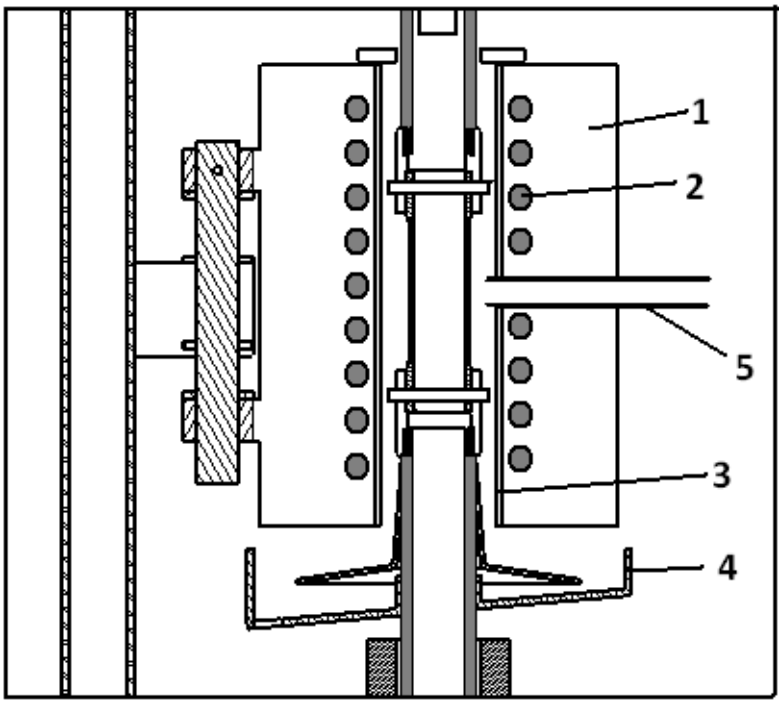

Figure 3.6 Portion of setup showing the split tube furnace, test piece and the feeder tube. 1. Refractory material, 2.Heating elements, 3.Stainless steel sleeves, 4.Powder tray, 5.Feeder tube

Figure 3.7 Split furnace used in the experiments

embedded heating elements are shown in **Figure 3.5**. The furnace has 750 watt power capable of reaching 1100^0C. The temperature control was achieved with a PID controller. The cross sectional view and the photograph of the vertical furnace were given in **Figure 3.6** and **Figure 3.7**.

As mentioned above, the furnace could reach to temperatures as high as 1100^oC, though the testing temperature was never more than 500^oC in the present study. The delivery of particles with high velocity air to the sample cools down the chamber atmosphere. So the use of more powerful furnace was helpful in maintaining the targeted temperature. Still to be able to maintain the temperature in the furnace, air must be preheated in the air conditioning unit (see below).

3.3 Particle Blower system

A schematic drawing of the particle blower used in the setup is given in **Figure 3.8**. The feeding of particles is based on a Venturi eductor that utilizes the kinetic energy of the high velocity air to create suction. Here air is fed into the system with a

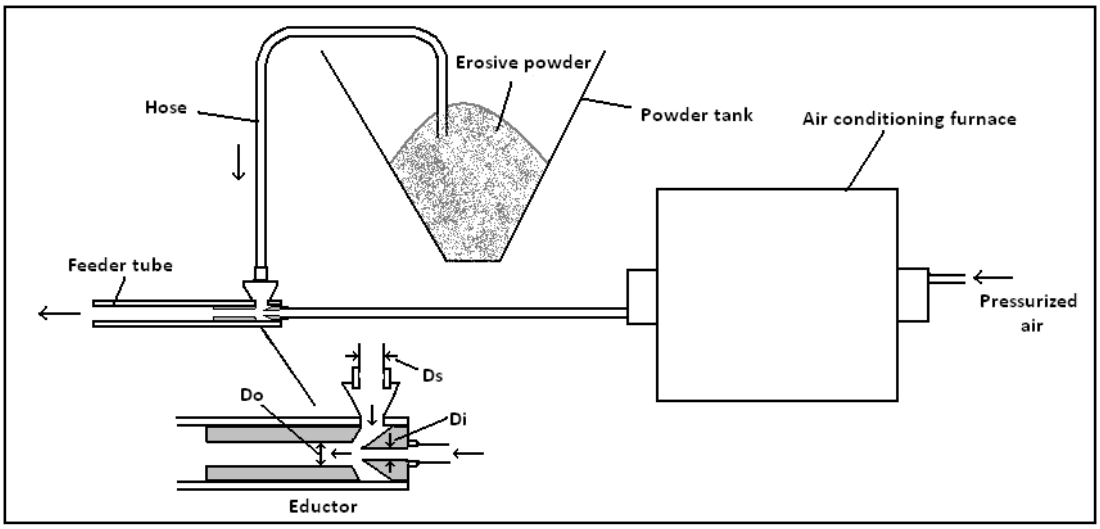

Figure 3.8 Schematic representation of the Particle Blower System (Di=Inlet diameter, Do=Outlet diameter, Ds=Diameter of hose for suction)

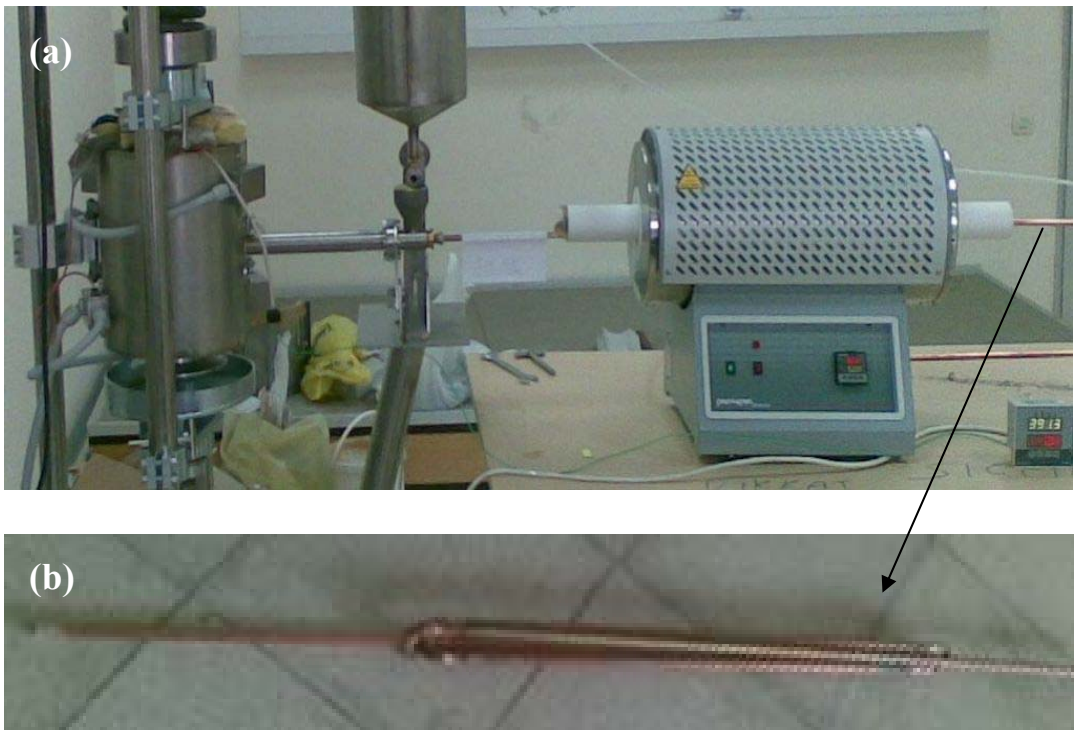

Figure 3.9 Photograph of **a)** Air conditioning furnace connected to the particle feeding system. **b)** Copper tube assembly.

compressor (0-8 bar) passing though a conditioning furnace. The system allows the delivery of air with velocity values of up to 50 m/s. The air fed through a thin walled (1 mm) copper tube (diameter 10 mm) was conditioned by circulating it in a simple tube furnace, **Figure 3.9.**

The furnace for air conditioning has a power of 1200 W and can be heated up to 1200^{o}C. The furnace was operated at temperatures less than 600^{o}C due to solder used in joining the copper tubes in the assembly, **Figure 3.9 (b)**.

The air, heated in the furnace, is fed to the eductor at a 4 mm (Di) diameter nozzle. The delivery diameter was 6 (Do) mm. The suction side (Ds) was adjustable from 6mm to 12 mm by changing the connecting hose. The feeding amounts in the order of hose diameter are 0.8g/min, 1.9g/min, 4.5g/min and 7.8g/min. It has been selected 10mm hose diameter. The powder blowing speed is 10±1m/s when the air is at room temperature.

Nozzle in the feeder tube is subject to intense erosion and as a result it was selected from B_4C. The nozzle needs to be changed after 400 hours of operation due to wear. The feeder tube is Al_2O_3 with the diameter of 15mm and the length of 35mm. Distance between the the tip of the feeder tube and the sample surface is 15mm.

Erosive particles blown on to the sample are diverted by the collar, firm fitted on to the sample, **Figure 4.3**. The powders falling from the collar are collected by the inclined tray (12), see **Figure 3.2**. This tray has a hole to which a cyclone or a vacuum system may be attached so as to collect the erosive particles.

Erosive materials used in the experiments are selected from oxides. Al_2O_3 and SiC are two possible candidates considered for this purpose. Based on the availability and the cost the choice was made for Al_2O_3. Chemical composition of the alumina powder is given in **Table 3.6**. As seen in the table, Al2O3 make up 90wt% of the powder. The other oxides comprise SiO_2, TiO_2 and Fe_2O_3.

Table 4.6 Composition of the erosive powder used in the experiments

Materials	Weight Conc.%
Al_2O_3	89.70
SiO_2	4.13
CaO	0.87
TiO_2	3.63
Fe_2O_3	1.67

Table 3.7 Erosive powder mesh analysis

Mesh size	Particle amount (%)
180 μm	1
250 μm	9
350 μm	34
420 μm	56

The powder has a mean particle size of 300μm. The particles are in the range 180-420μm (99%), **Table 3.7.**

3.4 Method of Experiments

Initial experiments with the set-up involved room temperature testing. These were carried out for the purpose of checking the reproducibility of the erosion taking place in the samples. Four samples were manufactured from 10CrMo9-10 tubes (EN 10216) [30], outside diameter of which was 38 mm with a wall thickness of 5 mm.

Duration in the experiments was 20 hours for each specimen. The erosion was measured by weighing the sample before and after the experiment, i.e. in terms of a material loss.

Having checked that the set-up produces a reliable result at room temperature, experiments were carried out at an elevated temperature. Experiment was conducted for 50 hours at 500^{o}C (±20^{o}C). This temperature was adjusted by considering the operating temperature of economizer tubes.

As mentioned above, in high temperature experiments furnace atmosphere was 500^{o}C (±20). In order to reach this temperature, furnace should be heated for 1 hour at 700^{o}C as tube specimen assembled in the system. Then, 5 hour experiment period the apparatus were closed and furnace atmosphere led to cool down for a while. After the cooling down, the powders were collected from the collection tray and system was prepared for following 5 hours experiment period by cleaning. Completing the 50 hour total experiment period the tube sample was ejected from the setup. During the ejection of the sample from the adaptor the oxide layer, formed during experiment, was peeled off. Therefore, the material loss comparison cannot be carried out correctly. Finally, the erosion amounts were compared by examining the boiler tubes thickness loss. For this reason, 30 mm long specimens were prepared. This sample preparation technique was explained in chapter 5 more detailed.

CHAPTER 4

RESULTS AND DISSCUSSION

Using the setup described in chapter 3, mainly three sets of experiments were carried out. These were i) reproducibility test carried out i) at room temperature, ii) at elevated temperature and iii) tests for economizer tubes.

4.1 Room Temperature Testing

Initial experiments with the setup involved room temperature testing. These were carried out for the purpose of checking the reproducibility of the test result, i.e. erosion taking place in the samples. Four samples were manufactured from 10CrMo9-10 tubes (EN 10216-2) [11], outside diameter of which, after machining, was 37 mm with a wall thickness of 5 mm, **Table 4.1.**

Experiment duration is 20 hours for each specimen. Erosion amount was measured as material loss. The measured material losses of tube specimens are given in **Table 4.2**. The values are quite close to each other indicating that the test results are quite reproducible. The average loss in the samples was 0.05 ± 0.007 g.

4.2 Elevated Temperature Testing

Having checked that the setup produces a reliable result at room temperature, experiments were carried out at an elevated temperature. For this purpose two 10CrMo910 boiler tube sample were tested.

Table 4.1 Chemical compositions of tube materials tested at high temperature according to TS EN 10216-2 standard [30]

Steel Name	C	Si	Mn	Cr	Mo	Ni	Al	Cu
P235GH	≤0.16	≤0.35	≤1.20	≤0.30	≤0.08	≤0.30	≤0.020	≤0.30
16Mo3	0.12-0.20	≤0.35	0.40-0.90	≤0.30	0.25-0.35	≤0.30	≤0.040	≤0.30
10CrMo9-10	0.08-0.14	≤0.50	0.30-0.70	2.00-2.50	0.90-1.10	≤0.30	≤0.040	≤0.30

Table 4.2 Weight measurements of 10CrMo910 materials at room temperature

	Before Tests(g)	After Tests(g)	Weight Loss(g)
1	707.44	707.39	0.05
2	701.28	701.22	0.06
3	694.38	694.34	0.04
4	677.51	677.46	0.05

For the elevated temperature testing, the measurement of erosion using the weighing method did not yield a reliable result. This was due to the oxidation of the sample which has led to weight gain, resulting a material loss value that was less than what was realized by erosion. Thus for the elevated temperatures, measurement of erosion by a weight loss was not suitable.

As a result, small specimens were prepared by cutting from the eroded boiler tube as shown in **Figure 4.1** and examined with a low magnification microscope. The specimen was 30mm in length and 10 mm in width. Thickness values were measured actually along the length of the cut piece.

Figure 4.1 High temperature test specimens used in experiments (a) Tested tube

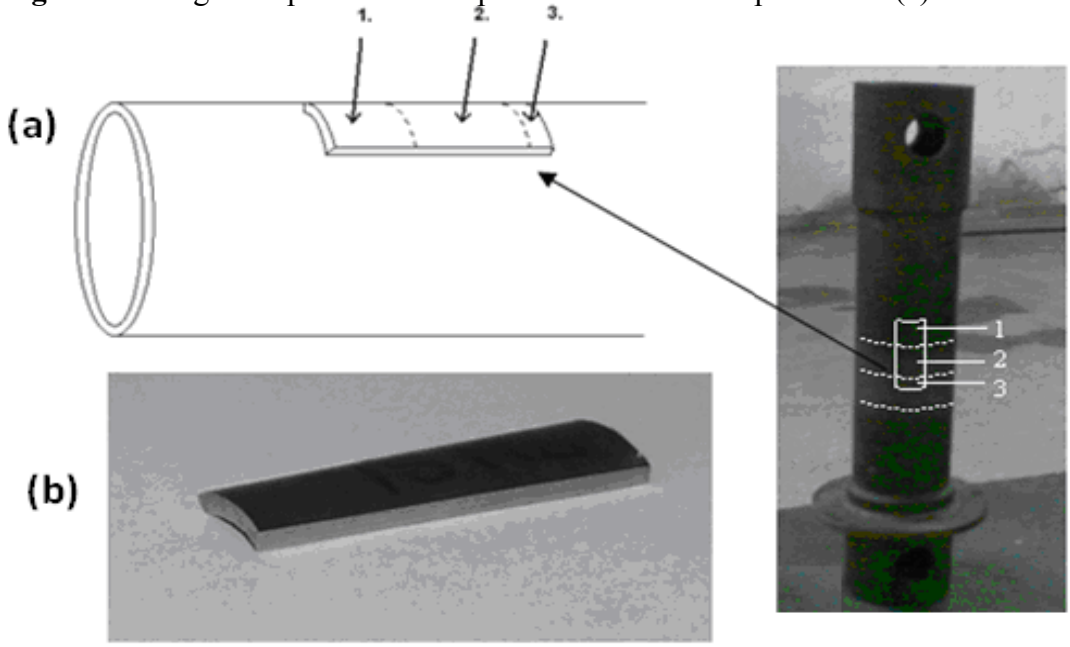

sample (on the right) and zones of prepared specimen (b) Specimen piece prepared for thickness measurements

Figure 4.2 shows the variation of the wall thickness of the sample in the eroded region. Initially uniform wall thickness reduces as one moves into the eroded region, reaching a maximum thickness loss value of 0.080 mm at the very center of the region. The variation of wall thickness is such that thinnest portion of the sample can be located quite easily. This shows that the maximum value of thickness loss can be determined at ease.

This thickness loss value may be used as a measure of material erosion. In fact the experiment reported above was repeated with a second sample, their test results are given in **Figure 4.3**, yielding a thickness loss value of 0.075 mm. The values are quite close to each other indicating that the thickness loss is nearly as reliable as the weight loss method used at room temperature.

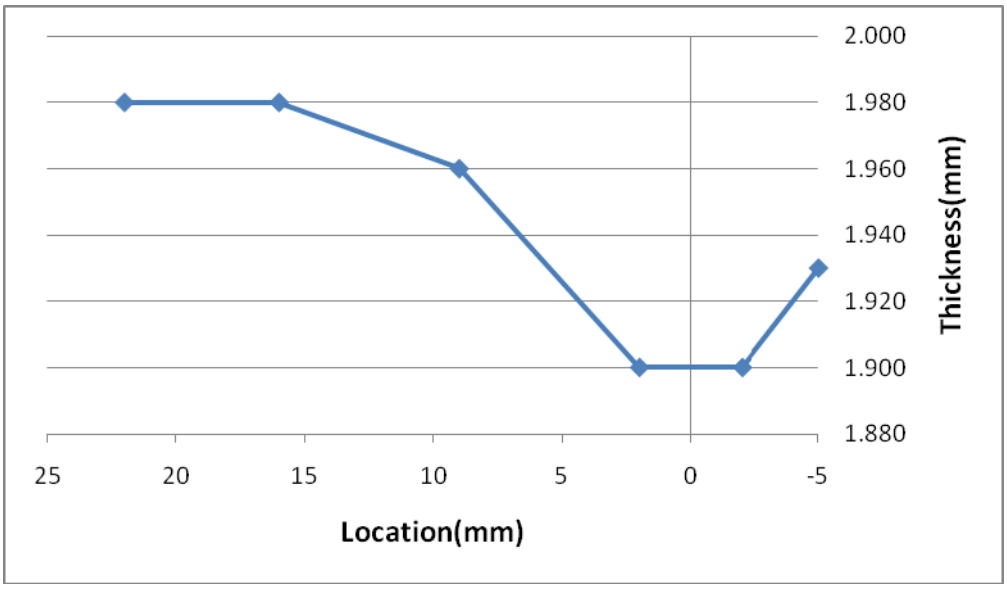

Figure 4.2 Thickness loss values of 1st 10CrMo910 boiler tubes eroded at high temperatures

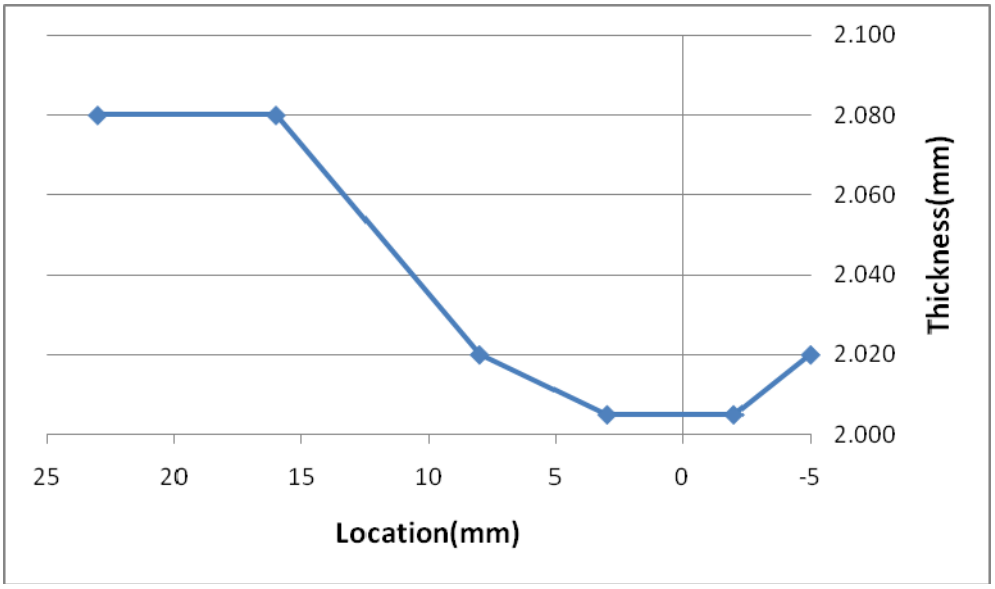

Figure 4.3 Thickness loss values of 2nd 10CrMo910 boiler tubes eroded at high temperatures

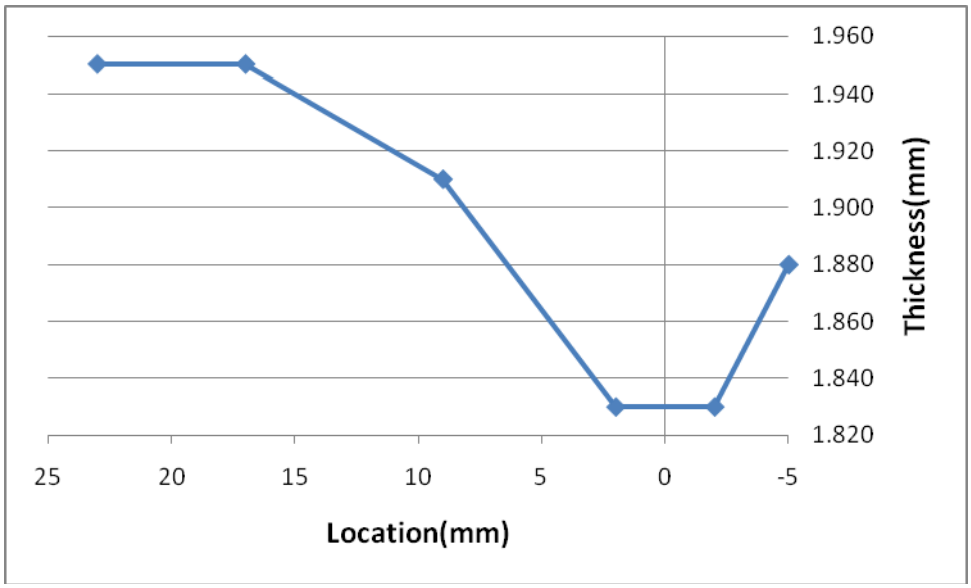

Figure 4.4 Thickness loss values of P235GH boiler tubes eroded at high temperatures

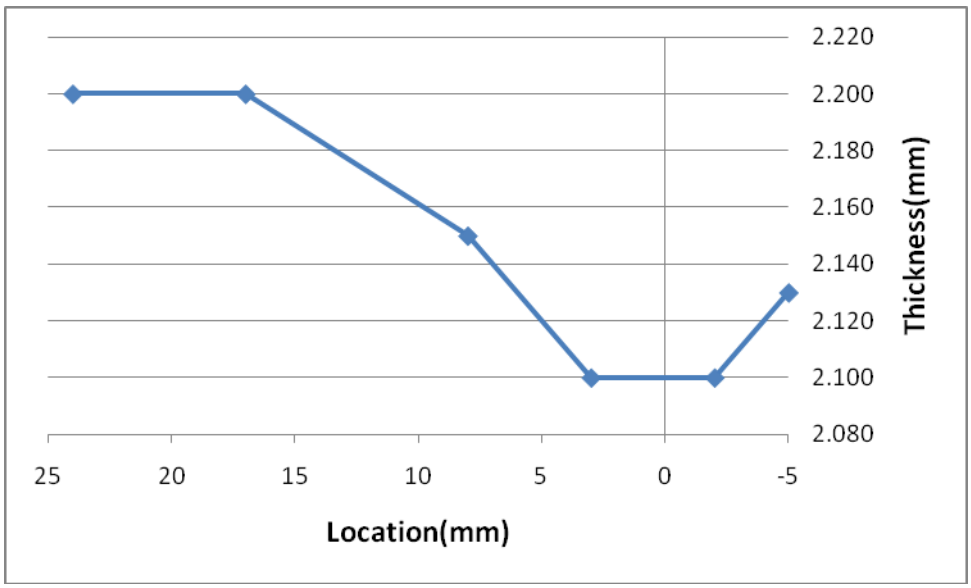

Figure 4.5 Thickness loss values of 16Mo3 boiler tubes eroded at high temperatures

4.3 Testing of Economizer Tubes

Finally we have used this setup to evaluate two economizer materials. These were P235GH and 16 Mo3 (EN 10216-2) given in **Table 4.1** tubes of 37mm diameter (wall thickness: approx. 2 mm). The erosion amounts were measured by thickness loss indicated in **Figure 4.4** and **Figure 4.5**. Testing carried out for 50 hours has yielded thickness loss values of 0.12 and 0.10 mm for P235GH and 16 Mo3 tubes respectively. This implies that in terms of erosion behavior that 16 Mo3 tubes are superior to P235GH ones.

According to the tests of economizer tubes 16Mo3 has better erosive durability than P235GH tubes. It has approximately %20 better erosive durability than P235GH.

CHAPTER 5

CONCLUSION

In this thesis, a test setup was developed for testing of boiler tubes used in thermal power plants. The setup simulates the conditions prevailing in the power plant and makes it possible the erosion behavior of the tubes to be evaluated on a relative basis. The setup is composed mainly of three components; i) a unit for sample loading system, ii) a furnace system to control and monitor the temperature of testing, and iii) a unit for blowing the abrasive particles.

In the loading system, the sample, simply a portion cut from the tubes, was connected to a mill with a pin coupling that can be rotated while being loaded with a spring. The set-up, as designed, is capable of applying tensile force values of up to 30 kN.

Heating system, as designed, would allow testing of boiler tubes up to a temperature of 650^{o}C. This was made possible with the use of split-tube furnace that houses the sample. The delivery of abrasive particles with air onto the sample cools down the chamber so to maintain the temperature, air was preheated in a conditioning unit.

The erosion was achieved by blowing the abrasives onto the rotating sample. This was made possible by an eductor system that utilizes the kinetic energy of the high velocity air to create suction onto the powder abrasives. The system allows the delivery of air with velocity values of up to 50 m/s. Erosive particles used in the experiments were a mixture of oxides, the greater portion of which was alumina.
The apparatus was tested at room temperatures using four samples from the same material (10CrMo910). Erosion was quite reproducible since the weight loss values

were on average 0.05g with a standard deviation of 0.007g. At elevated temperature, the measurement of erosion using the weighing method was not possible due to the oxidation of the sample. It was shown that the erosion in such cases could be measured by a thickness loss value which was also reproducible. Finally, the set-up was used for testing of two economizer materials; P235GH and 16Mo3. This has shown that 16Mo3 had a better performance than P235GH against erosion where the rate of erosion differed by 20%.

Tubes tested for economizer clearly indicates the usefulness of the setup designed in the present work. This test could be extended for tubes, which are subject to erosive wear, in other regions of the boiler. The setup would allow an easy testing of tube coatings which may be used to minimize erosion.

REFERENCES

[1] International Energy Outlook 2010, U.S. Energy Information Administration, July 2010, http://www.eia.doe.gov/oiaf/ieo/pdf/0484(2010).pdf, 2 August 2010.

[2] Elektrik Üretim AŞ. 2009 Elektrik Üretim Sektör raporu, http://www.enerji.gov.tr /yayinlar_raporlar/Sektor_Raporu_EUAS_2009.pdf, May 2010.

[3] Kömür(Linyit) Sektör Paporu 2009, Türkiye Kömür İşletmeleri Kurumu Genel Müdürlüğü, Ankara 2010, http://www.tki.gov.tr/dosyalar/KömürSektörRaporu2009 .pdf, May 2010.

[4] Electric Power Research Institute, Field Guide: Boiler Tubes Failure Report, Theory Section 3-4-5, Appendix A, 2004.

[5] Elektrik Üretim AŞ. Gölbaşı Laboratory, Failure Analysis Results (unpublished study), 2008

[6] J.B. Kitto and S.C. Stultz, Steam: its generation and use, Selecter Color Plates, Eddition41, Babcock & Wilcox Company, 2005.

[7] Engineering drawing of Çayırhan thermal power plant (taken from the thermal power plant)

[8] Angela V. Manolescu and P. Mayer, Structure a8nd Composition of Protective Magnetite on Boiler Tubes, paper No. 174, presented at Corrosion/80 (National Association of Corrosion Engineers), Chicago, Illinois, 3-7 March 1980.

[9] H. A. Grabowski and H. A. Klein, Corrosion and Hydrogen Damage in High Pressure Boilers, 2nd Annual Educational Forum on Corrosion, National Association of Corrosion Engineers, September 1964.

[10] John P. Hurley, Steven A. Benson, Thomas A. Erickson, Sean E. Allan, Jay Bieber, Project Calcium Topical report, pp1, Energy and Environmetal Research Center, Grand Forks, North Dakota, September,1992.

[11] Robert D. Port, Harvey M. Herro, The Nalco Guide to Boiler Failure Analysis, McGraw-Hill Company,1991, pp135, 201-202.

[12] R. Viswanathan, Damage Mechanism and Life Assessment of High Temperature Components, ASM International, Third printing, 1995, pp194-195.

[13] Boiler Tube Analysis:Reduce Future Boiler Tube Filures E101-3153, The Babcock & Wilcox Company, www.babcock.com

[14] Dünya Enerji Konseyi Türk Milli Komitesi (DEK-TMK), Temiz Kömür Teknolojileri Çalışma Grubu, 16 Mart 2010, Ankara.

[15] M. Şahin, Effects of Fly Ash and Desulphogypsium on the Strength and Permeability Properties of Çayırhan Soil, December 2005.

[16] B. Lindsley, k. Stein and A.R. Marder, The design of a high-temperature erosion apparatus for studying solid particle impact, Energy Research Center, Lehigh University, Bethlehem, USA, 5 December 1994.

[17] L. Zhang, V. Sazonov, J. Kent, T. Dixon, V. Novozhilov, Analysis of boiler-tube erosion by the technique of acoustic emission Part I. Mechanical erosion, Wear 250, 2001, pp 762-769

[18] M. Suckling, C. Allen .Critical variables in high temperature erosive wear, Wear 203-204, Cape Town, South Africa, 1997, pp 528-536.

[19] Buqian Wang, Seong W. Lee, Erosion–corrosion behaviour of HVOF NiAl–Al2O3 intermetallic-ceramic coating, Wear 239, USA, 1 July 1999, pp83-90.

[20] Girish R. Desale, Bhupendra K. Gandhi, S.C. Jain, Effect of erodent properties on erosion wear of ductile type materials, Wear 261, 4 April 2006, pp 914–921.

[21] Tylczak, T. Adler, and J. Rawers. Abrasion and Erosion Testing of Materials Used in Power Production From Coal ,J Albany Research Center, USA, 2003

[22] Noriyuki Hayashi, Yoshimi Kagimoto, Akira Notomi, Yasuyuki Takeda, Koji Katoba, Development of new testing method by centrifugal erosion tester at elevated temperature, Wear 258, 22 December 2003, pp 443–457.

[23] T.A. Daniel Sagayaraj, S. Suresh, and M. Chandrasekar, Experimental studies on the erosion rate of different heat treated carbon steel economizer tubes of power boilers by fly ash particles, International Journal of Minerals, Metallurgy and Materials Volume 16, Number 5, October 2008, pp 53.

[24] D.O. Moumakwa, K. Marcus, Tribology in coal-fired power plants, Tribology International 38, 2005, p 805–811.

[25] Mete402 Design Project Report prepared by group T7 4th year studenst of Metallurgical and Materials Engineering Department of Middle East Technical University, 2007

[26] Joseph Edward Shigley, Charles R. Mischke, Mechanical Engneering Design, Fifth addition, McGraw-Hill Book Co., Singapore, 1989, pp332.

[27] Compression Spring End Design, http://www.roymech.co.uk/Useful_Tables/ Springs/Springs_helical.html, 2.11.2009.

[28] ASTM Sandards, Chrome Silicon - ASTM A 401 Spring Wire Properties

[29] Stainless steel AISI 316, http://www.substech.com/dokuwiki/doku.php ?id=stainless_steel_aisi_304 26.06.2008.

[30] Institute of Turkish Standards, TS EN 10216-2.Seemless steel tubes for pressure purposes- Technical delivery conditions – Part:2 Non-alloy steel tubes with specified elevated temperature properties, Ankara 2010, in Turkish.